THERMAL PERFORMANCE INVESTIGATION OF A WATER COOLING PVT COLLECTOR WITH DIFFERENT COOLING SUBCHANNELS

2023
MASTER THESIS
MECHANICAL ENGINEERING

Zainab Mohammed Sellab AL MAMOORI

Thesis Advisor
Assist. Prof. Dr. Enes KILINÇ

THERMAL PERFORMANCE INVESTIGATION OF A WATER COOLING PVT COLLECTOR WITH DIFFERENT COOLING SUBCHANNELS

Zainab Mohammed Sellab AL MAMOORI

Thesis Advisor
Assist. Prof. Dr. Enes KILINÇ

T.C.
Karabuk University
Institute of Graduate Programs
Department of Mechanical Engineering
Prepared as
Master Thesis

KARABUK
September 2023

I certify that in my opinion the thesis submitted by Zainab Mohammed Sellab AL MAMOORI titled “THERMAL PERFORMANCE INVESTIGATION OF A WATER COOLING PVT COLLECTOR WITH DIFFERENT COOLING SUBCHANNELS ” is fully adequate in scope and in quality as a thesis for the degree of Master of Science.

Assist. Prof. Dr. Enes KILINÇ .....
Thesis Advisor, Department of Mechanical Engineering

This thesis is accepted by the examining committee with a unanimous vote in the Department of Mechanical Engineering as a Master of Science thesis. Sep.1, 2023

Examining Committee Members (Institutions)	Signature
Chairman : Prof . Dr. Mehmet ÖZKAYMAK (KBU)	.....
Member : Assist. Prof. Dr. Enes KILINÇ (KBU)	.....
Member : Assist. Prof. Dr. Fatih UYSAL (SUBU)	.....

The degree of Master of Science by the thesis submitted is approved by the Administrative Board of the Institute of Graduate Programs, Karabuk University.

Assoc. Prof. Dr. Zeynep ÖZCAN .....
Director of the Institute of Graduate Programs

"I declare that all the information within this thesis has been gathered and presented in accordance with academic regulations and ethical principles and I have according to the requirements of these regulations and principles cited all those which do not originate in this work as well."

Zainab Mohammed Sellab AL MAMOORI

ABSTRACT

M. Sc. Thesis

THERMAL PERFORMANCE INVESTIGATION OF A WATER COOLING PVT COLLECTOR WITH DIFFERENT COOLING SUBCHANNELS

Zainab Mohammed Sellab AL MAMOORI

Karabuk University
Institute of Graduate Programs
The Department of Mechanical Engineering

Thesis Advisor:
Assist. Prof. Dr. Enes KILINÇ
September 2023, 69 pages

This computational study was conducted to study the impact of cooling sub channels on the PVT collector's thermal performance using ANSYS Fluent. Four geometrical cases have been included in the study, with different dimensions of sub cooling channels (10×10) mm, (12.5×12.5) mm, (15×15) mm, and (20×20) mm. The effect of channels dimensions, temperature distribution, velocity distribution, pressure drop, heat transfer and the figure of merit (FoM) with deferent Re numbers has been discussed in the study. The simulations manifested that the photovoltaic system's average temperature surface decreased with the increasing of sub channels cooling dimensions and Re number. The pressure drop decreases as the dimensions of sub cooling channels increased. The surface average temperature of the PVT modules was 38.49°C, 36.88°C, 35.92°C, and 34.65°C for the four cases, respectively in the Re number range of 920 to 2275. The pressure drop for the same cases in the same range of Re number were 30.86 Pa, 19.23 Pa, 13.2 Pa, and 6 Pa, respectively.

Keywords **:** PVT collectors, cooling channels, Reynolds number, pressure drop.
Science Code : 91408

ÖZET

Yüksek Lisans Tezi

FARKLI SOĞUTMA KANALLARINA SAHİP SU SOĞUTMALI BİR PVT KOLLEKTÖRÜNÜN ISIL PERFORMANSININ İNCELENMESİ

Zainab Mohammed Sellab AL MAMOORI

Karabük Üniversitesi
Lisansüstü Eğitim Enstitüsü
Makine Mühendisliği Anabilim Dalı

Tez Danışmanı:
Dr. Öğr. Üyesi Enes KILINÇ
Eylül 2023, 69 sayfa

Bu hesaplamalı çalışma, ANSYS Fluent kullanılarak paralel soğutma kanallarının PVT kollektörleri,termal performansı üzerindeki etkisini incelemek için yapılmıştır. Alt soğutma kanalları (10×10) mm, (12.5×12.5) mm, (15×15) mm ve (20×20) olmak üzere farklı boyutlarda Solidworks yazılımı ile yapılan dört geometrik modül çalışmaya dahil edilmiştir. mm. Kanal boyutlarının etkisi, Sıcaklık Dağılımı, Hız Dağılımı, soğutma kanallarındaki basınç düşüşü, Isı Transferi ve farklı Re sayısı ile liyakat rakamı (FoM) çalışmada tartışılmıştır. Simülasyonlar, PV modül yüzeyinin ortalama sıcaklığının, alt soğutma boyutlarının ve Re sayısının artmasıyla azaldığını ortaya koymaktadır. Alt soğutma kanallarının boyutları arttıkça basınç düşüşü azalır. PVT modüllerinin yüzey ortalama sıcaklığı, 38.49°C, 36.88°C, 35.92°C ve 34.65°C'dir. 920 ila 2275 Re sayısıaralığında sırasıyla dört vaka. Aynı Re sayısı aralığındaki aynı durumlar için basınç düşüşü sırasıyla 30.86 Pa, 19.23 Pa, 13.2 Pa

ve 6 Pa idi.

Anahtar Kelimeler : PVT kollektörleri, soğutma kanalları, Reynolds sayısı, pressure drop.

Bilim Kodu : 91408

ACKNOWLEDGMENT

I would like to express my sincere thanks and appreciation to Assist. Prof. Dr. Enes KILINÇ for his support, time, guidance, valuable information, and interest in supervising my thesis throughout my academic journey. I also thank to the head of the department of mechanical engineering, Prof. Dr. Kamil ARSLAN, and his staff for the assistance they provided.

My thanks and gratitude to my husband, for his support and encouragement throughout my study period.

I would like to thanks my family and everyone who has supported me .

CONTENTS

Page

Page

LIST OF FIGURES

Page

Page

LIST OF TABLES

Page

SYMBOLS AND ABBREVITIONS

T : Temperature (K)

P : Pressure (pa)

T_i : Inlet temperature

T_o : Outlet temperature

RE : Renewable Energy

FoM : Figure of merit

SE : Solar energy

PV : Photovoltaic

PVT : Photovoltaic thermal

CFD : Computational fluid dynamics

T_s : Temperature of the surface (k)

K : Thermal conductivity ($W\backslash m.k$)

A : Cross-sectional area (m^2).

h : Heat transfer coefficient ($W/m^2.k$).

m : Mass flow rate (kg/s).

c_P : Specific heat ($J/kg\ K$)

G : Solar irradiance (W/m^2)

$\dot{Q}$: Heat transfer rate (W)

Re : Reynolds number

ρ : Density (kg/m^3)

ΔP : Pressure drop (Pa)

D_h : Hydraulic diameter (m)

v : Velocity (m/s)

μ : Dynamic viscosity ($pa.s$)

L : Length (m)

W : Width ($_m$)

PART 1

INTRODUCTION

1.1. WORLD ENERGY SCENARIO

Energy is required by technological applications in practically every field, including agriculture, industry, and domestic activities. As time goes on, there will be an even greater increase in the amount of energy needed for meeting the demands. Energy supplies become less readily available as the population grows and energy demand rises. The 22nd century is predicted to see the complete exhaustion of fossil fuels, which we currently use extensively[1]. The burning of fossil fuels has produced residues that have contributed significantly to climate change and environmental pollution. As a result, numerous researchers from around the world have expressed interest in studies on renewable energy sources that do not hurt the environment [2]. Energy produced from natural resources, like solar, wind, tides, geothermal, bioenergy, and hydropower, is referred to as renewable energy (RE). In contrast to conventional energy sources (such as oil, coal, and natural gas), renewable energies have little to no negative environmental effects and don't produce any waste greenhouse gases. Thus, it would seem that the best and most efficient method to handle environmental issues and worries regarding the sustainability of energy sources is through the use of renewable energies [3]. The REN21 report states that net installations of nuclear and fossil fuel power capacity combined are currently being surpassed by net additions of renewable power generation capacity. By the end of 2021, 40 nations around the world had at least 10 GW of installed renewable power capacity, up from 24 nations only ten years earlier. As seen in Figure 1.1, producing electricity from wind and solar photovoltaic is less expensive than doing so from brand-new coal-fired power facilities in the majority of nations [4].

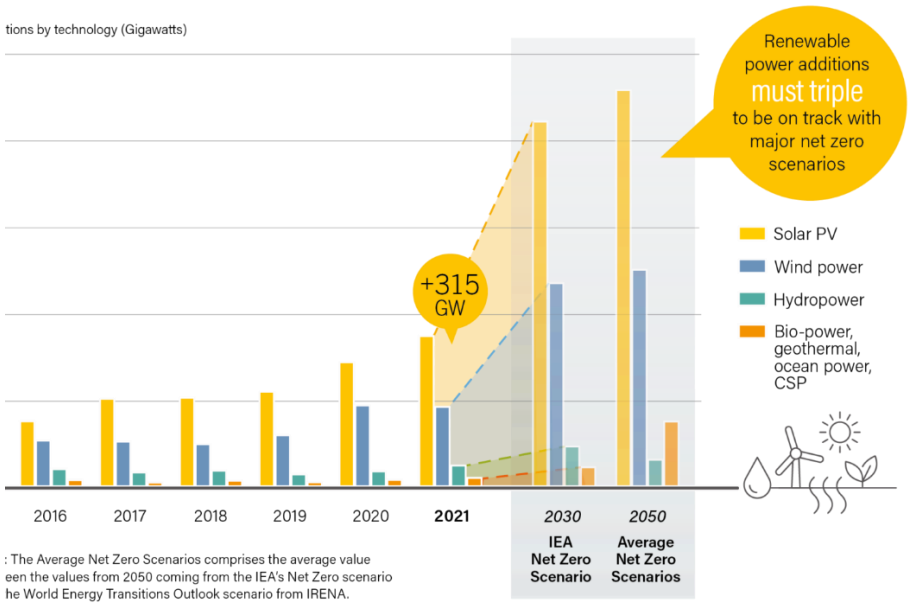

Figure 1.1. Annual addition of renewable energy capacity 2016-2021 [4].

1.2. SOLAR ENERGY

One of the most important renewable energy forms is solar energy (SE). Clean, safe, and inexpensive energy may be produced without endangering the environment by utilizing the light and heat that the sun provides [2]. The annual solar flux is almost 100 times more than the annual global energy consumption, which indicates that if just 1% of incident solar radiation was harvested, it would be enough to meet everyone's energy demands [5]. Sun is a continuous fusion reactor with an output of 3.8×10^{20} MW. This energy is radiated in all directions, and the Earth intercepts 1.7×10^{14} kW of radiation that is emitted [6]. Solar energy is infinitely renewable and has almost no negative environmental effects. This energy could be captured using a variety of methods, such as PVs, which converts the light directly into electricity, solar thermal technologies, which heat the water and then convert it into other forms of energy, and concentrated solar power, which concentrates the solar energy by lenses to intense energy beams that could be utilized for heating water as well as providing conventional energy solutions. The enormous solar energy amount, which is available, makes it a highly alluring electricity source. Longer time, developing affordable, infinite, and sustainable solar energy technologies will have several advantages. By depending on a local, limitless, and largely import-independent

resource, it will provide energy security for states, improve sustainability, decrease pollution, minimize expenses associated with mitigation, and maintain lower-than-normal fossil fuel prices [5].

1.3. PV SYSTEMS

PV technology is used to turn sunlight into electricity. The term is made up of the words "photo" and "voltaic," which both refer to light and electricity. Semiconductors are used to create solar cells and PV cells, which could convert the solar light into electricity [7]. The photovoltaic effect is the process by which solar cells convert light into electrical power. Edmond Becquerel demonstrated the photovoltaic effect for the first time in 1839. These solar cells are constructed from two different types of semiconductors that are linked together to form a p-n junction. An electric field is produced in the junction when these two various semiconductor kinds are combined. As shown in Figure 2, this generated field promotes the movement of positively charged particles, holes to the negative side, and negatively charged particles, electrons to the positive side [8,9,10].

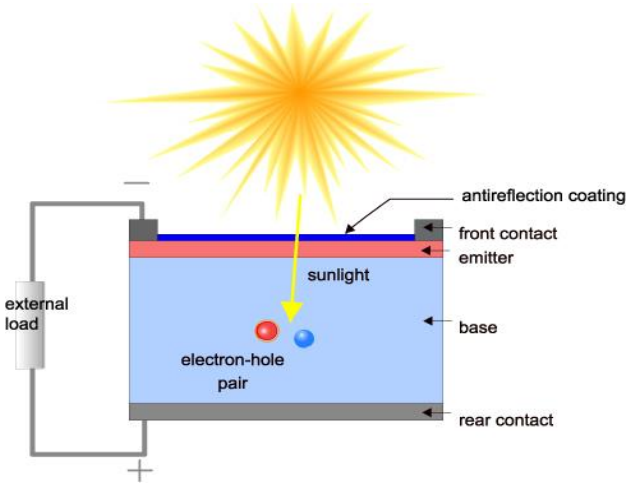

Figure 1.2. Sectional view of a solar cell [9].

A variety of materials can be used to make photovoltaic cells, but silicon, which is abundant on earth and has semiconducting characteristics, is frequently utilized in solar cells. Depending on the quality and case material of the silicon, PV cells are produced and marketed in three different categories, as depicted in Figure 1.3 [10].

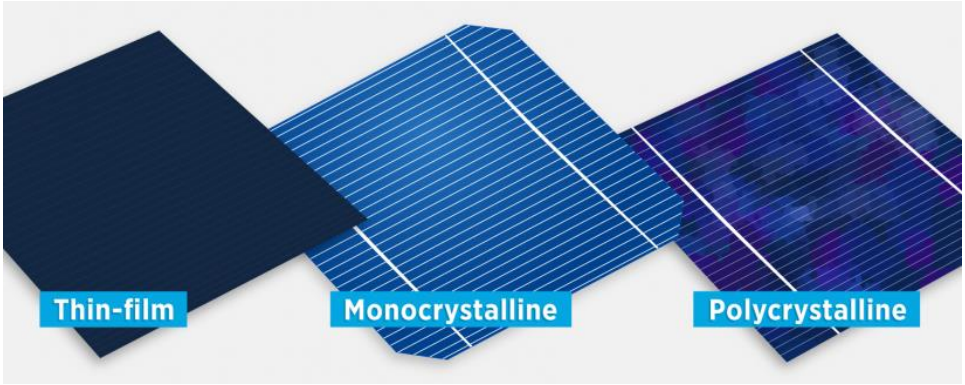

Figure 1.3. Types of solar panels [11].

1.4. PVT SYSTEMS

Solar energy is converted into electrical energy by PV panels. Maintaining the operational temperature of solar panels is important [12]. A rise in temperature results in the panels heating up and a reduction in electrical efficiency. Preventing overheating is essential for avoiding a decline in electrical efficiency. To avoid overheating, ducts or pipes are placed on the back side of PV panels. The PVT systems' collector is made up of this structure. They use the system's collector to simultaneously convert the solar energy into electrical and thermal energy. PV cells, absorber plates, channels, and thermal insulation are the PVT system's main parts. PV cells are typically attached to a solar collector's thermal absorber to create PVT systems. Thermal absorbers are therefore the solar cells' complement in a PVT system since they absorb solar energy and use it. The thermal and electrical efficiency of PVT system are highly influenced by the thermal absorber. Since the thermal absorber is primarily situated between the fluid and the PV module, it plays a crucial part in transferring heat from the PV layer to the fluid. The type of solar collector utilized in the PVT system determines the thermal absorber model. Aluminum and copper are the two main materials used in thermal absorbers [13]. A glass cover can be installed on the PV cells. Glazing decreases heat loss and increasing the thermal efficiency. At the same time, the electrical efficiency rises when the PVT systems do not contain glass because of the higher solar radiation intensity. A general schematic illustration of PVT systems is revealed in Figure 1.4 [14].

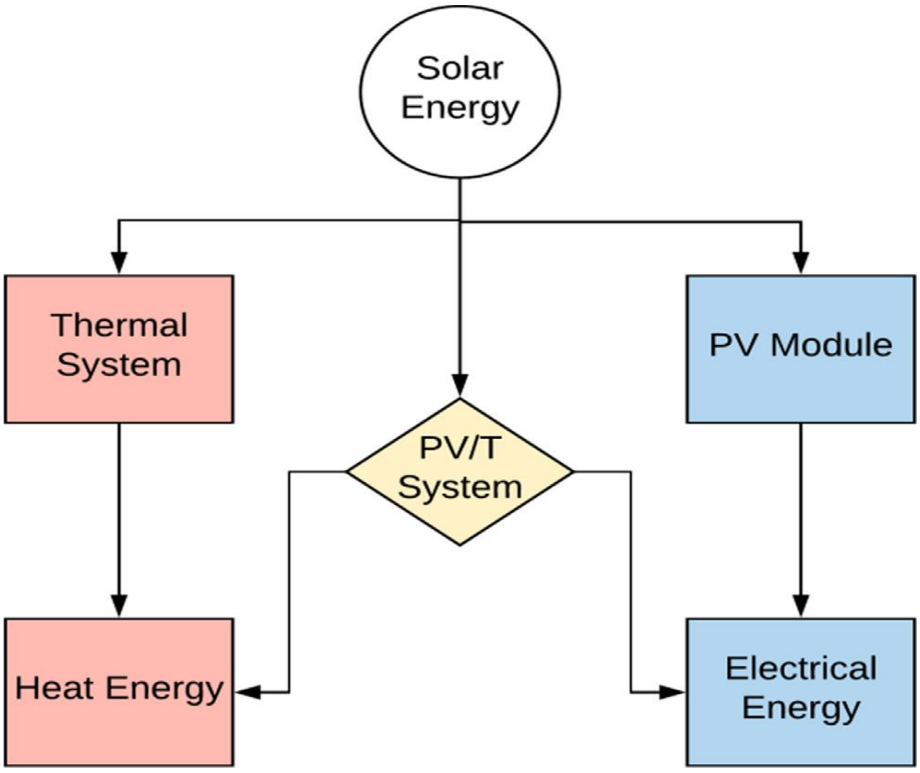

Figure 1.4. Solar technology diagrams [15].

Thus, the heat removal from PV panels via uniform cooling approaches is required to keep the temperature of the PV panel within the manufacturer's operating range. For the thermal management and performance enhancement of PV/PVT panels, different cooling techniques are utilized. There are various ways to provide uniform cooling, including:

- Airflow cooling
- Jet impingement cooling
- Liquid Immersion cooling
- Liquid/water cooling
- Heat pipe cooling
- Thermoelectric cooling
- PCM cooling
- Micro channel cooling [16].

Based on the design and type of PV cell, the type of fluid flow, and whether or not solar radiation is concentrated, the PVT systems could be divided into various types. According to that, the PVT collectors include PVT liquid flow collectors, PVT collectors with air circulating through them, and PVT collectors that combine water and air, as illustrated in Figure 1.5 [17].

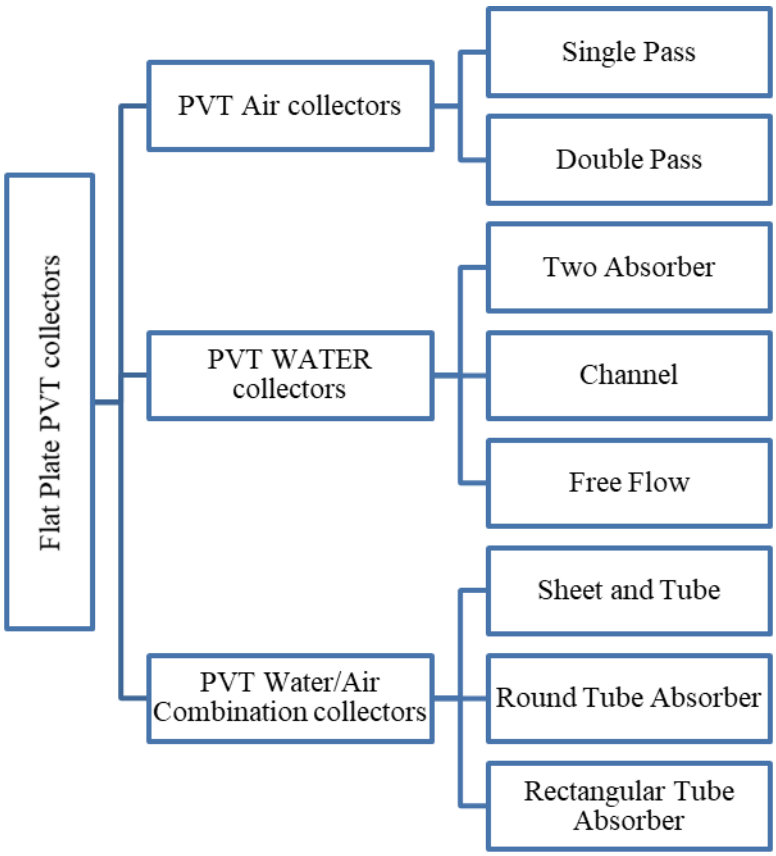

Figure 1.5. Classification of PVT Collectors [18].

The heat removal medium that is utilized for cooling the solar cells could be air, water, or refrigerant. The heat produced by the PV panel is absorbed by the water-based PVT collector, as displayed in figure 1.6 (a), which circulates water as the heat transfer fluid. Due to its higher thermal conductivity and heat capacity, the water type collector is more efficient and useful than the air type collector [19].

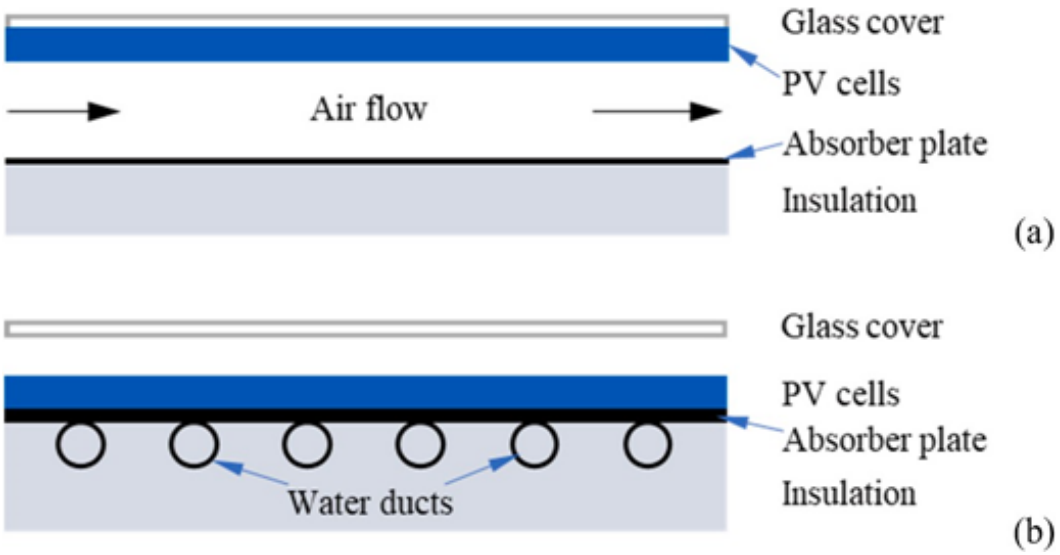

Figure 1.6. Flat plate collector (a) air-based PVT and (b) water-based PVT [20].

In a PVT system with air-based is evinced show in Figure 1.6 (b). utilized to maintain the PV module's temperature at the ideal range, allowing for high power output. Moreover, the heating system is used for ventilation, space heating and drying, etc. [21].

1.5. THESIS PLAN

The aims of this thesis is to improve the thermal performance of PVT collector, decreases the temperature of the photovoltaic module and make the photovoltaic cell temperature more uniform. by creating simulation model of photovoltaic thermal (PVT) collector with change in dimensions of sub channel channels for four cases.

Chapter 2 presents literature review for experimental and theoretical studies for different types of cooling techniques employed in PVT collector and their impact on system efficiency.

Chapter 3 developing simulation for four model of PVT system by applying computational fluid dynamics (CFD) techniques and utilizing ANSYS fluent software, based on continuity, momentum, energy equations and study the effect of

change in sub channel channels dimensions on thermal performance on PVT collector.

Chapter 4 presents and discusses all the obtained results of the Simulation carried out on the PVT collector to demonstrate the effect of altering the dimensions of the sub channels on system performance.

Chapter 5 summarizes and displays all of the findings from this investigation.

PART 2

LITERATURE REVIEW

This section demonstrates the experimental and theoretical studies that have used different techniques to cool a photovoltaic thermal system. After renewable energy systems became a reality and the demand for them increased, researchers continued to improve their efficiencies.

Rejeb et al. improved electrical and thermal efficiencies of solar collector by developing a new photovoltaic thermal/collector. The effect of arrangement (thermal resistance between the cooling fluid and absorber plate, antireflective and low-emissivity coating, and enhanced exchange surface area between the cooling fluid and the flat plat exchanger) on the new PV/T collector was also analyzed and studied. The simulation results showed that adding an anti-reflective coating to a solar module improves both electrical and thermal performance. The heat transfer between the PV module and the thermal absorber is improved. Higher thermal and electrical efficiency are obtained for the recommended PV/T collector (73%, 15.4%) as compared to the basic PV/T collector (58%, 13.7 %) [22].

Arslan et al. designed, manufactured, and inspected a new finned air fluid PV-thermal collector kind, performed experimental and numerical analyses with varying values of the mass flow rates and conducted energy and exergy analyses for thermal and electrical efficiencies. Results depicted that the photovoltaic cooling improved the electrical efficiency by about (0.42%). The average electrical and thermal efficiency of the PV thermal system were (13.56% and 37.10%), respectively, at a mass flow rate (0.031087 kg/s) and (13.98% & 49.5%) for mas flow rate (0.04553 kg/s) [23].

Elbreki, et al. enhanced the photovoltaic efficiency by combining planar reflector and back plate extended surface depending on the effects of lapping fin height, fin spacing, number of fins, wind speed, and solar radiation. Results illustrated that the increase of fin pitch from 20 mm to 60 mm caused decreasing the number of fins from 20 to 10. In turn, it increased the temperature of photovoltaic module from 44.13°C to 54.01°C. The temperature of photovoltaic module without the cooling reached 64.30°C, which at the same time, with 18 lapping fins and 27.7 mm fin pitch, the temperature of photovoltaic module decreased to 39.73°C, which enhanced the electrical efficiency to 11.20% as compared with the bare photovoltaic 9.81% with a difference of temperature that equals 24.57°C at 1000 W/m^2. The lapping fins have a superior performance in the reduction of the temperature of photovoltaic module [24].

A. F. Muftah et al. investigated the passive cooling performance of the concentrated photovoltaic module and employed two different novel designs for the passive fin heat sink, which are longitudinal and lapping, to distinguish the optimum design based on the height of the fin, fin thickness, tilt angle, fin pitch, and the number of fins. Results revealed that the passive cooling with the lapping fins indicates the optimal performance with an average temperature of the photovoltaic module 24.60℃ lower compared to the reference photovoltaic module, and thus, the electrical efficiency and output power reached 10.68% and 37.1 W, respectively [25].

Boumaaraf et al. developed two numerical models, evaluated them using MATLAB environment, combined the numerical simulation and experimental investigation, and compared the typical photovoltaic generator and photovoltaic thermal collector performance between a classical PV generator and a water glazed PV/T collector. The results displayed that the overall thermal efficiency could be as high as (74.20%) for the photovoltaic thermal collector system, while it was (18.43%) for the photovoltaic generator [26].

Choubineh et al. performed an experimental investigation on an air-cooled photovoltaic system that has been equipped with phase change materials. Their goal was to analyze the influence of the utilization of the phase change materials on the

heat transfer performance at natural convection and forced air convection. Experimental results evinced that the panel's temperature decreased to (4.30°C, 3.40°C, 3.60, and 3.70°C) in a natural flow, decreasing the panel temperature, and forced high-velocity, medium-velocity, and low velocity, respectively. When equipped with phase change materials sheets additionally, reducing the temperature results in augmenting the electrical efficiency and outlet power; in turn, results in a considerable rise in the natural and forced convection situations [27].

Javidan et al. investigated photovoltaic cooling modules utilizing multi-nozzle jet impingement cooling; this study focused on the influence of the number of nozzles, nozzles diameter, and dimensionless nozzle on the photovoltaic gaping, upon the general system performance. Results manifested that any increase in the liquid mass flow rate improves the photovoltaic electrical efficiency. The photovoltaic output power module was also improved by the number of nozzles. The mean surface temperature of photovoltaic module reduced from (63.95℃ to 33.68℃) when applying perfect properties. The maximum improvement in the output power of system was (47.67%) at the perfect conditions. The optimal temperature uniformity achieved for the least nozzle to the photovoltaic spacing (5.0 mm), minimal nozzle diameter (1.0 mm), and maximal number of nozzles (24) [28].

Khaled et al. presented a hybrid PV/T solar collector system in Duhok city that was the subject of numerical and experimental examination over the course of seven months. This study included various measurements of temperature, wind speed, water mass flow rate, and solar intensity. Transient processes were simulated using a 1D mathematical model with constant thermo physical characteristics and heat transfer coefficients. The implicit finite difference approach was used for solving the equations relating to energy conservation. The estimation of thermal and electrical energy as well as thermal, electrical, and total efficiency was included in the results. The PV/T collector's overall efficiency reached its best point in May 2019 (72.01%), and it reached its lowest point in January 2019 (63.1%). In comparison with a PV solar collector system, the electrical efficiency of the cooling approach increase to roughly 3% [29].

Keen et al. developed an experimental study of twisted tape inserted in an evacuated tube solar water heater. The experimental Results elucidated that the heat transfer and outlet temperature of working fluid in the tube with a twisted tape inserted were more than in the evacuated tube without the twisted tape insert since the average efficiency of the evacuated tube solar water heater with twisted tape was 68.35% ,while for the evacuated tube solar water heater without the twisted tape, It was 59% [30].

Selimli et al. achieved an experimental and numerical comparison and the investigation of PV module as well as PV thermal collectors based on the thermodynamics' first and second laws. The experimental results were compared with the numerical results, which were obtained from the CFD. Results indicated that the electrical efficiency of photovoltaic module was equal to the overall efficiency of about 7.96%. Electrical, thermal, and overall energy efficiency values were 9.74%, 29.08%, and 38.82%, respectively for the photovoltaic thermal serpentine collector, and those for the photovoltaic thermal channeled collector were 49.68%, 10.19%, and 59.88%, respectively. The exergy efficiency of the photovoltaic module, photovoltaic thermal serpentine collector, and photovoltaic thermal channel collector was determined at approximately 4.63%, 10.64%, and 11.53%,respectively [31].

Poredoš, et al. presented the experimental and numerical energy and exergy performance evaluations of the solar thermal, PV and PV thermal modules dependent roll-bond heat exchangers with various channel geometries, parallel, bionic, and serial. Results viewed that the lowest temperature at outlet water inside the absorber was at the bionic absorber, and the bionic indicated lower pressure losses. The simulation results showed the maximum solar-to-electrical efficiency (14.50%) in bionic absorber. The photovoltaic thermal module achieved the highest average electrical and exergy efficiencies as coupled with a bionic absorber plate [32].

Rosli et al. carried out computational fluid dynamics simulations for different designs of absorber tube, u-flow, spiral, and serpentine designs to study and compare the electrical, thermal, and total efficiency levels of the Photovoltaic thermal collector for different absorber tube designs. Effects of mass flow rate on the performance of

the PV thermal were specified, and the surface to surface (S2S) radiation model was applied. The results demonstrated that in (the 0.0005 kg/s and 0.005 kg/s) range, the u-flow, serpentine, and spiral design of photovoltaic thermal obtained the maximum thermal efficiency (at 0.005 kg/s) that were 21.02%, 22.62%, and 22.960%, respectively. In terms of electric efficiency, the u-flow design controlled attained 11.780%, the maximum ele1ctrical efficiency of the three designs (at 0.0050 kg/s). Spiral design and serpentine had the same electrical efficiency (11.67%). at 0.0050 kg/s. All three photovoltaic designs attained the highest total efficiency at 0.0050 kg/s in the range between 0.00050 kg/s and 0.0050 kg/s. At 0.0050 kg/s, the spiral designed indicated the highest thermal efficiency, 34.630%, serpentine design, 34.290%, and u-flow design, 32.80% [33].

Zhou et al. established a 3-D thermal model of water-cooled flat panel photovoltaic thermal collector with the serpentine flow tube utilizing a finite element approach to study distribution of the temperature of a photovoltaic thermal collector at serpentine tube. The effects of serpentine cooling tube configuration on the distribution of the temperature were investigated. From the simulation results, the optimum design of cooling channels should comprehensively regard the pressure drop and channels' effects [34].

Misha et al. developed and studied a novel dual oscillating absorber copper pipeline flow depending on the photovoltaic water system in its design, to enhance the electric performance and get useful heat, in turn, enhance the general efficiency by applying CFD simulation and experimental investigation. The CFD results were validated with the experimental results. Results have appeared that the maximal average thermal efficiency of photovoltaic thermal system was 59.60%. The maximum mean value of the electric efficiency of the photovoltaic panel and photovoltaic thermal water system were 10.860% and 11.710%, respectively, at a mass flow rate equal to 6 LPM. The photovoltaic thermal electrical, thermal efficiency and output power increased with the mass flow increment. The thermal efficiency increased with the mass flow rate increase, the level of solar irradiation, and decreasing the difference between the inlet and outlet temperatures of water. when increasing the mass flow rate, the temperature of cell decreased [35].

Salem, et al. introduced experimental studies for the photovoltaic thermal system performance using an aluminum cooling plate with helical and straight channels. Results depicted that the increases in the average electrical efficiency of (17.70% - 38.4%) compared with the non-cooled panels for a range of the flow rate of (0.25L/min – 1 L/min). The mean thermal efficiency increased from (31.60%) to (47.20%) for straight channels and from (34.6%) to (57.9%) for helical arrangement. And, the average exergy efficiency rose from (11.10%) to (12.90%) for straight channels and from (11.5%) to (13.5%) for helical configuration. The power of the water pump in the two arrangements didn't exceed 3.30% of the converted electrical power, whereas the increasing in the received electrical power was 30% compared to the non-cooled cell power [36].

Kazem et al. presented the architecture of a grid-connected water-based PV/T, together with the performance results from tests conducted outdoors in Oman's climate. This research showed the findings of the impact of environmental factors and solar irradiance on and standard PV/T collectors and PV panels by concentrating on the electrical performance regarding the system throughout 3 days of testing. The suggested PV/T exhibited higher electrical performance over the traditional PV throughout the period of examination, with a steady increase in the electrical efficiency. Around 67 WP and 18.90 V, respectively are the system's peak electrical output and voltage. The PV/T panel's average power was found to be 6% higher compared to that of a regular photovoltaic panel [37].

Engin et al. developed a mathematical model and inspected the electrical and thermal efficiency of a hybrid photovoltaic thermal collector system prototype. The electrical efficiency was enhanced by decreasing the cell temperature of photovoltaic module. This is why a photovoltaic thermal system has been modeled and then created by utilizing a thermal collector located at the lowest of the PV panel since the surplus heat and solar radiation are the input of thermal collector. Coating the absorber plate with TiO_2 increased the thermal output by 10%. The coated absorber plate and transparent solar module by TINOX increased the hybrid system thermal yield [38].

Khelifa et al. presented a mathematical model to study a photovoltaic panel system for producing the electricity combined with a thermal system for water heating. The system is formed by sheet and tube placed under the surface for extracting heat from the photovoltaic module and cooling cells and to increasing the electric efficiency. Results indicated that the outlet temperature of fluid in the system reached the temperature of 39°C that showed again in the produced thermal energy [39].

Michael et al. introduced an experimental study on a new PV thermal water-based collector created by the lamination of photovoltaic cells on copper thermal absorber. The modification decreased thermal the resistance by (9.93%), which enhanced the heat transfer from photovoltaic cells to the fluid. Experiments were carried out with and without glazing, with various stagnant conditions and water mass flow rates, and with and without load conditions and thermal stress tests. The results revealed that (87.52%) overall efficiency was obtained in the presence of glazing and (a 0.1 kg/s) mass flow rate [40].

Shen et al. established a heat transfer theoretical model in PV thermal collectors with various parallel cooling channels to evaluate the parallel cooling channels' effect of the thermal performance of PV/T collectors. The numerical results appeared that at ten sub-channels, the pressure drop of the cooling channels was minimal. In the meantime, the temperatures of PV modules were low and uniformly distributed. As well, the I-type setting of the inlet and outlet was an optimal option because the cooling channels' pressure drop was low and thermal performance of the photovoltaic thermal collector was very good. As the diameter ratio between the main channel and sub-channels increases, the PV module temperature decreases and becomes distributed more uniformly. The figure of the merit of cooling channels with (D/d = 4) might be higher than that with (D/d = 2) by 50% [41].

Abdin et al. presented a novel photovoltaic thermal (PV/T) collector employing a heat storage tank at the back of a module and an electrical resistance to improve the thermal output during the periods of peak demand. This inquiry used modeling and CFD to construct a dynamic model of the system's operation. The simulation demonstrated the viability of models and designs. The simulation facilitated

determining the relationship among the insulating thickness, quantity supplied, fluid characteristics, and serpentine pipe material. The results indicate that the temperature of the components increases with the addition of an air gap between the cover of glass and the solar cell component, the thickness of the insulator is a crucial design factor, with a maximum of 0.10 m, the temperature increases with the use of copper as a component material, water diluted with glycol is a good alternative because it is less expensive and has better heat transfer than pure water, and recycled engine oil improves the thermic efficiency. [42].

Bria et al. evaluated the ability of a PV/T water supply and a flat absorb design composed of aluminum tubes to cool the solar panels, using computational fluid dynamics for climate-based numerical analysis in Morocco. It was compared to an uncooled PV module to determine the efficiency of the PV/T system. The effectiveness of a moisture absorber (PV/T) for solar panel cooling was investigated. This project aimed to increase the efficiency of photovoltaic panels by better-utilizing waste heat. Analyzed beneath the photovoltaic module was an aluminum absorber with circular water tubes. Using computational fluid dynamics (CFD) simulations, the impact of a few variables on the efficiency of photovoltaic (PV) panels was examined. The diameter of the inner tube, the rate of water introduction, and the input and outlet configurations were all variables. The T's cooling approach improved the thermal and electrical efficiency by decreasing the PV/temperature ratio. After cooling, the median temperature of the photovoltaic panel was 26.8 ℃. The PV cell temperature decreased with tube diameter and water speed. In just one of the four investigated cooling arrangements, the temperature of the PV cell decreased from the five-tube-by-five configuration, and it helped maintain a steady temperature for the photovoltaic panels. The diameter of the inner tube, the velocity of the water intake, and the water inlet/exit design all affected the PV/T efficiency [43].

Chen et al. developed a 3-D thermal and hydro-dynamic model for constructal tree-shape mini channel heat sink. The heat and fluid flow in the constructal heat sink with a hydraulic inlet diameter of 4 mm were analyzed numerically, taking under consideration the conjugate heat transfer in channel walls. Temperature uniformity, pressure drop, and COP of constructal tree-shaped heat sink were assessed and then

compared to the ones of corresponding conventional serpentine flow pattern. Results indicated that the constructal tree-shaped mini channel heat sinks have important benefits when compared to the conventional serpentine flow patterns in pressure drop and heat transfer. The weak and strong heat flow may be allocated with high effectiveness in the tree-shaped flow structures, where the local pressure loss that results from the confluence flow is higher when compared to than that which results from the difference flow. The experimentally measured distribution of temperature and drop of pressure are in agreement with the numerical simulations. Additionally, the aluminum constructal tree-shaped mini channel heat sink has been fabricated for the purpose of conducting the verification experimentation of [44].

Su et al. demonstrated the PV/T solar collector's performance with dual channels for various fluids. By the comparison of 4 PV/T collectors with various fluids, the electrical and thermal parameters of the PV/T solar collector, such as the temperatures regarding the solar cell and outlet fluids, thermal power efficiency, and electric power production efficiency were examined. The most effective PV/T collector in terms of thermal and electrical performance has been discovered to be water-water cooled. The most hot water could be produced by a PV/T collector that is water-water cooled. In the air-water situation, the water's temperature is at its highest. The PV/T collector that is air-air cooled has the potential to produce the most hot air at the highest temperature. Additionally, it has been discovered that an increase in the mass flow rate of water and the distance between the higher and lower pipes improves the overall efficiency of water-cooled PV/T collectors [45].

Liang et.al. showed a solar concentrating photovoltaic-thermal (CPV-T) module for building louver. This type of module is intended for providing buildings with both heat and electricity through absorbing solar radiation in their vertical spaces. A PV-T module was utilized in conjunction with a specially created concentrating blade for a louver. Incident sunlight can converge on a solar cell thanks to the concentrating blade, producing electricity, through using thermal fluid to remove and collect the heat produced by the solar cell. The focusing blade's high-efficiency PV/T working range was 20-70º, and it was intended to operate with a solar incidence angle of 0-90º. To show the features of the concentrating blade, optical simulations were run. At

an incidence angle of 20º, the geometrical concentration ratio was at its highest value of 2.96. The geometrical concentration ratio remained above 2 throughout a broad range of incident angles between 12.5º and 52.5º. Lastly, tests were done to see how well the CPV-T module performed electrically and thermally. The findings showed that over the entire day of experiment, its total efficiency could remain over 55% for almost 5 hours without tracking [46].

Dubey et al. installed and tested two different varieties (Types B and A) of commercially available PV/T modules. The PV module in Type A was enclosed by mono-crystalline Silicon solar cells and integrated with tube-and-sheet thermal collector, while the photovoltaic module in Type B was enclosed by multi-crystalline Silicon solar cells as well as integrated with parallel-plate thermal collector. Thermal and PV efficiencies were used to evaluate the PV/T modules' performance. The tests were conducted under typical day climatic circumstances at two different flow rates (0.03 kg/sec and 0.06 kg/sec). Fundamental energy balance equations and design factors were used to validate the modules' thermal performance. In order to better understand the heat flow pattern throughout the PV/T modules, the temperature across their various layers was measured. The average thermal efficiency and photovoltaic efficiency for Type A and Type B PV/T modules were 40.70% 11.80%, 39.40% and 11.50%, respectively. When PV modules' electrical efficiency was evaluated without and with thermal collector, it was discovered that the PV/T modules' average photovoltaic efficiency was roughly 0.4% greater than the standard PV module [47].

Salman et al. a proposed new design for a cooling system and then numerically examined it is design. Water serves as the working fluid through the photovoltaic panel's rear chamber. Porous media were used for filling the chamber, which will improve the convection heat transfer. With the use of Navier Stokes equations, the ANSYS program simulated the incompressible steady-state flow of water. To study the impacts of solar radiation, mass flow rate, and porosity on the PV module's performance, several circumstances for the cooling fluid flow field and the temperature distribution regarding the PV panel were provided. The findings displayed that the addition of porous media decreases this module's average

temperature from 9°C to 14°C. When the flow rate increases, the heat transfer is significantly improved. An experimental study was conducted for comparing the experimental results with the numerical ones in order to validate the work that has been provided. With an error ranging between 2.9% and 10.9% for the cooling with the porous media and between 4.5% and 8.5% for cooling without porous media, such comparisons demonstrated a good agreement [48].

Prasetyo et al. modeled the SiO2, TiO2, and Al2O3 nanofluids and water heat transfer fluids to cool PV solar cells utilizing different riser designs on PV/T collectors. The thermal and electrical efficiency regarding a PVT collector system were studied by altering the radiation intensity, collector design's shape, kind of the fluid that has been employed, and fluid flow rate. The heat transmission process between photovoltaic cell layer and the fluid was simulated using an ANSYS model. The layout of a rectangular riser collector with water evinced the maximum electrical efficiency at the value of 11.87%. The configuration regarding a semi-circular riser filled with water had the best level of the thermal efficiency, 121%. The electrical efficiency of the photovoltaic solar cells was unaffected by utilization of a riser collector arrangement in a PV/T collector system. Each riser collector arrangement shape's working fluid had an impact on how well the photovoltaic solar cells generated the electricity. Water was used and it produced efficiencies up to 3.27% higher than any of the other nanofluids that were evaluated. Considerable electrical efficiencies for photovoltaic solar cells were attained while employing a fluid mass flow rate of 0.5 kg/s in every one of the riser collector configurations and fluid types, with maximum efficiency being 11.98%. The resultant thermal efficiency, for instance, was 82.70%. As a result, in various riser collector arrangements, the mass flow rate of working fluid could have an impact on the electrical efficiency of the PV solar cells [49].

Huide et al. described the solar thermal, photovoltaic, and hybrid photovoltaic/thermal simulation models and carried out experiments to validate the simulation results. The performance of the three household solar systems was projected. Energy comparisons between three solar systems utilized in different parts of China were also investigated. Results manifested that, among the solar PV,

thermal, and hybrid PV/thermal systems, a hybrid PV/thermal system might have the highest potential for lowering the energy consumption for an urban residential building with limited available area for installation. Additionally, a system with PV and hybrid PV/thermal modules could produce maximum net yearly electricity output for a rural home with a considerable amount of available space. The area of the installation of hybrid PV/thermal collectors is mostly dependent on the building's hot water usage [50].

Pang et al. simulated and tested under the real-world working conditions, a thermal model of a hybrid PV/T system with a polycrystalline silicon PV module and an aluminum thermal collector. With an inlet mass flow rate of 0.034 kg/s and a heat flux of 700 W/m2, the pressure, temperature, and velocity distributions over the PVT module were shown. Experimental results that supported the thermal model's predictions regarding the PV/thermal module's performance without and with a coolant elucidated that the PV/T module's temperature was nearly 20°C lower than the comparable PV module. With coolant circulated at a 100 L volume, the p-Si PV/T module's electrical energy and output power rose by no less than 2% and 10%, respectively. The PV/T module's output power and electrical energy looked to be around 7% and 5%, respectively, while it ran without coolant circulation [51].

Kiwan et al. modified the standard solar chimney system to increase its economic viability. Installation of a water pool to cool PV panels and enable the system to produce freshwater were the two primary improvements. The inclusion of photovoltaic system will result in increasing the system's overall electricity generation. In order to evaluate the viability of both the standard and modified systems, a mathematical model was created. It was discovered that the modified system's deployment factor was 4.37% whereas the traditional system's utilization factor was 0.51%. The variables contributing to optimal utilization factor were found via parametric analysis. The submerged PV panels performed better when placed nearer to the chimney. According to the findings, the suggested system generates 45.35% more electricity yearly compared to a standalone photovoltaic system set up in the same place. Additionally, the results of the sensitivity analysis suggest that the height of the chimney has the greatest impact on the system utilization factor. In

other words, the factor of utilization is larger as the chimney gets higher. The economic research comes to the conclusion that the system produces freshwater at a cost of 1.60 US$/$m^3$, which is 46.30% less expensive than that produced by other comparable systems. Additionally, compared to a typical solar chimney, the economic indicators for the suggested system demonstrate the enhancement [52].

Salari et al. quantitatively studied the PV and PV/T systems' performance for the impact of dust deposition density. A monocrystalline silicon PV module's whole structure was modeled for the two systems. It was investigated how the different system characteristics affect the performances of the dusty as well as the clean PV modules and PV/T systems. Solar radiation intensity, coolant inlet temperature, ambient temperature, and coolant inlet velocity were among the parameters examined. The obtained data portrayed that the electrical efficiency of PV module decreased by 26.36% in the case where the dust deposition density on its surface increased from 0 g/ m^2 to 8 g/ m^2. Additionally, the electrical and thermal efficiencies of the PV/T system decreased by 16.11% and 26.42%, respectively, as the dust deposition density on its surface increased from 0 g/m^2 to 8 g/m^2.Furthermore, the simulation findings exhibited that the effect of the factors under consideration has a greater impact on the clean solar system compared to the dusty system. Two correlations for the decline in thermal and electrical output as a dust deposition density function have also been put out [53].

PART 3

THEORATICAL BACKGROUND (METHODOLOGY)

In this part, a numerical method is used for the photovoltaic thermal (PVT) water collector with four different dimensions of cooling channels to evaluate the effect of the structure of the cooling sub channels on the thermal performance of PVT collector. Modules are created through simulation using computational fluid dynamics (CFD) Finite volume method is used for obtaining the solutions in the fluid simulation system. The shape geometry is created with the SolidWorks 2022 software, the mesh is created with the Gambit 2.4.6 program, and the numerical simulations are solved with the ANSYS Fluent (2022) program.

3.1. COMPUTATIONAL FLUID DYNAMIC (CFD)

The science of computational fluid dynamics (CFD) involves solving a set of governing mathematical equations numerically to predict fluid flow, heat transfer, mass transfer, and related phenomena. These equations are the conservation of mass, conservation of momentum, conservation of energy and effects of body forces [54]. With each solution displaying a rich tapestry regarding numerical methods, mathematical physics, user interfaces, and cutting-edge visualization methods, CFD is now developing into a potent and omnipresent tool in many industries [55]. Methods like CFD could be used to achieve findings that are near to reality while reducing the time and cost required for development and research. In-depth analysis is provided by simulation analysis, which cannot be achieved through experimentation. For instance, using CFD simulation, it is feasible to determine the temperature distribution inside the equipment [56]. CFD became a more practical approach for delivering effective design solutions due to the recent advancements in computing the effectiveness and falling prices of CFD software packages [57]. It is recognized as a validating numerical method that can simulate separated particles by

monitoring each particle's motion in the flow. Furthermore, it is capable of simulating complex fluid flows with quantitative and qualitative analysis of the changing flow field in both space and time [58]. The finite volume approach is one of many CFD technologies that are available [59–61].

3.2. MATHEMATICAL MODEL

Governing equations including the continuity equation, momentum equation, and energy equation were employed to obtain the results and determine the optimal model for this study.

Continuity equation:

$$\frac{\partial u}{\partial x}+\frac{\partial v}{\partial y}+\frac{\partial w}{\partial z}=0 \tag{3.1}$$

Where u, v and w represent the water's velocities along the x, y and z axes, respectively.

Momentum equation:

$$\nabla\cdot(\rho u\vec{u})=-\frac{\partial p}{\partial x}+\frac{\partial \tau_{xx}}{\partial x}+\frac{\partial \tau_{yx}}{\partial y}+\frac{\partial \tau_{zx}}{\partial z} \tag{3.2}$$

$$\nabla\cdot(\rho v\vec{u})=-\frac{\partial p}{\partial y}+\frac{\partial \tau_{xy}}{\partial x}+\frac{\partial \tau_{yy}}{\partial y}+\frac{\partial \tau_{zy}}{\partial z} \tag{3.3}$$

$$\nabla\cdot(\rho w\vec{u})=-\frac{\partial p}{\partial z}+\frac{\partial \tau_{xz}}{\partial x}+\frac{\partial \tau_{yz}}{\partial y}+\frac{\partial \tau_{zz}}{\partial z}+\mathrm{F} \tag{3.4}$$

Where p is the water's pressure (pa), τ is the viscous stress, $F=\rho g$ is the gravitational force, ρ is the water's density [62,63].

Energy equation:

$$\frac{\partial(\rho uT)}{\partial x}+\frac{\partial(\rho vT)}{\partial y}+\frac{\partial(\rho wT)}{\partial z}=\frac{\partial}{\partial x}\left(\frac{k}{c_P}\frac{\partial T}{\partial x}\right)+\frac{\partial}{\partial y}\left(\frac{k}{c_P}\frac{\partial T}{\partial y}\right)+\frac{\partial}{\partial z}\left(\frac{k}{c_P}\frac{\partial T}{\partial z}\right) \tag{3.5}$$

Where T is the temperature of the water, k is the thermal conductivity, c_P is the heat transfer coefficient of the water.

The Fourier's law, as shown in equation, expresses steady-state conduction heat transfer. [64].

$$Q = -KA(\frac{dT}{dX}) \tag{3.6}$$

Where Q is the conductive heat transfer rate (W), K is the thermal conductivity $(W\backslash m.k)$, A is the cross-sectional area (m^2), $(dT\backslash dx)$ is the temperature slope in the direction of heat flow.

The Newton's law of cooling, which is represented in equation, is used to express the convective heat transfer:

$$Q = hA_s(T_s - T_\infty) \tag{3.7}$$

Where Q is the convective heat transfer rate (w), h is convection heat transfer coefficient $(W/m^2.k)$, A is the heat transfer surface area (m^2), T_s is the temperature of the surface (k), T_∞ is the temperature of the fluid (k).

The heat transfer rate can be expressed as:

$$\dot{Q} = \dot{m}C_P(T_o - T_i) \tag{3.8}$$

Where $\dot{Q}$ is the rate of heat transfer (W), $\dot{m}$ is the mass flow rate (kg/s), c_P is the specific heat capacity of water $(J/kg.K)$, T_i is the inlet water temperatures (K), T_o :is the outlet water temperatures (K).

The Pressure drop ΔP can be expressed as:

$$\Delta P = f\frac{L}{D}\frac{\mu V^2}{2} \tag{3.9}$$

Where D is the hydraulic diameter (m), ΔP is the pressure drop (Pa), v is the average velocity (m/s), ρ is the density of water $(kg/m3)$, μ is dynamic viscosity $(pa.s)$, L is the length of the cooling channel (m).

Figure of merit (FoM) is the evaluation performance of the cooling channels given as

$$FoM = \frac{\dot{Q}}{m\Delta P} \tag{3.10}$$

Where $\dot{Q}$ is the rate of heat transfer (W),$\dot{m}$ is the mass flow rate (kg/s), ΔP is the pressure drop (Pa).

Reynolds number:

$$Re = \frac{\rho v D_h}{\mu} \tag{3.11}$$

Where ρ is the density of fluid (kg/m^3), V is the velocity of fluid (m/s), μ is a dynamic viscosity of the fluid $(pa.s)$ [65].

3.3. PHYSICAL MODEL AND BOUNDARY CONDITION

Four geometrical models have been done in this study, in order to assess the impact of a parallel cooling channel's dimension altering on the thermal performance of the PVT water collector. ANSYS Fluent was used to analyze the performance of the PVT water collector. Solid works software (2022) was used to create a three-dimensional design of the system with regard to the numerical analysis. As shown in figure 3.1, the collector of the PVT system utilized in the numerical analysis is made of glass, silicon solar cells, aluminum absorber plates, and two main channels that collect ten cooling parallel copper sub channels between them. The dimensions and characteristics of PVT collector are presented in Table 3.1. In the numerical simulation, a laminar three-dimensional steady model was utilized. Water was used as a cooling fluid. The fluid flow is laminar, with a (Re < 2300) and a range of Re (920,1200,1520, 1600, 1850, 2275). Water enters the parallel channel at T_{in} = 300 K.

The atmosphere's pressure, Pout = 0 Pa, was used to keep a constant water pressure at the output. A 1000 W/m^2 heat flux was applied on the surface glass of the PVT water collector. The PVT system's side and bottom surfaces were insulated. As a result, the bottom and side surfaces of the PVT collector were considered to be adiabatic (heat flux=0).

Table 3.1. The dimensions and properties of the PVT system.

Material	**Density** (kg/m^3)	**Thermal conductivity** $(W/m.K)$	**Specific heat** $(J/kg.K)$	**Thickness** (mm)
Glass	2450	2	500	4
Silicone	2329	148	700	6
Aluminum	2700	160	900	1
Copper	8978	387.6	381	1
water	998.2	0.6	4182	

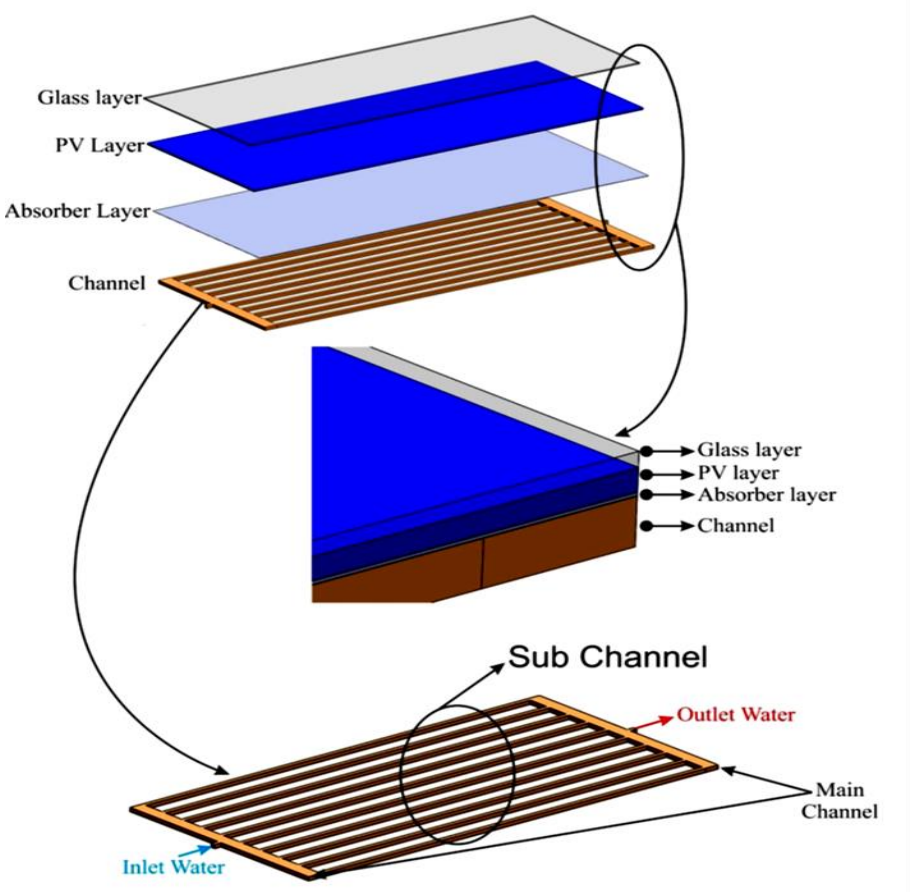

Figure 3.1. Structure of PVT system

The length (L) and the width (W) of the (PVT) water collector were determined as (1305 mm × 630 mm) respectively as show in Figure 3.2. The four models are change in sub channel dimensions as show in Figure 3.3. Table 3.2 presents the dimensions of sub channels.

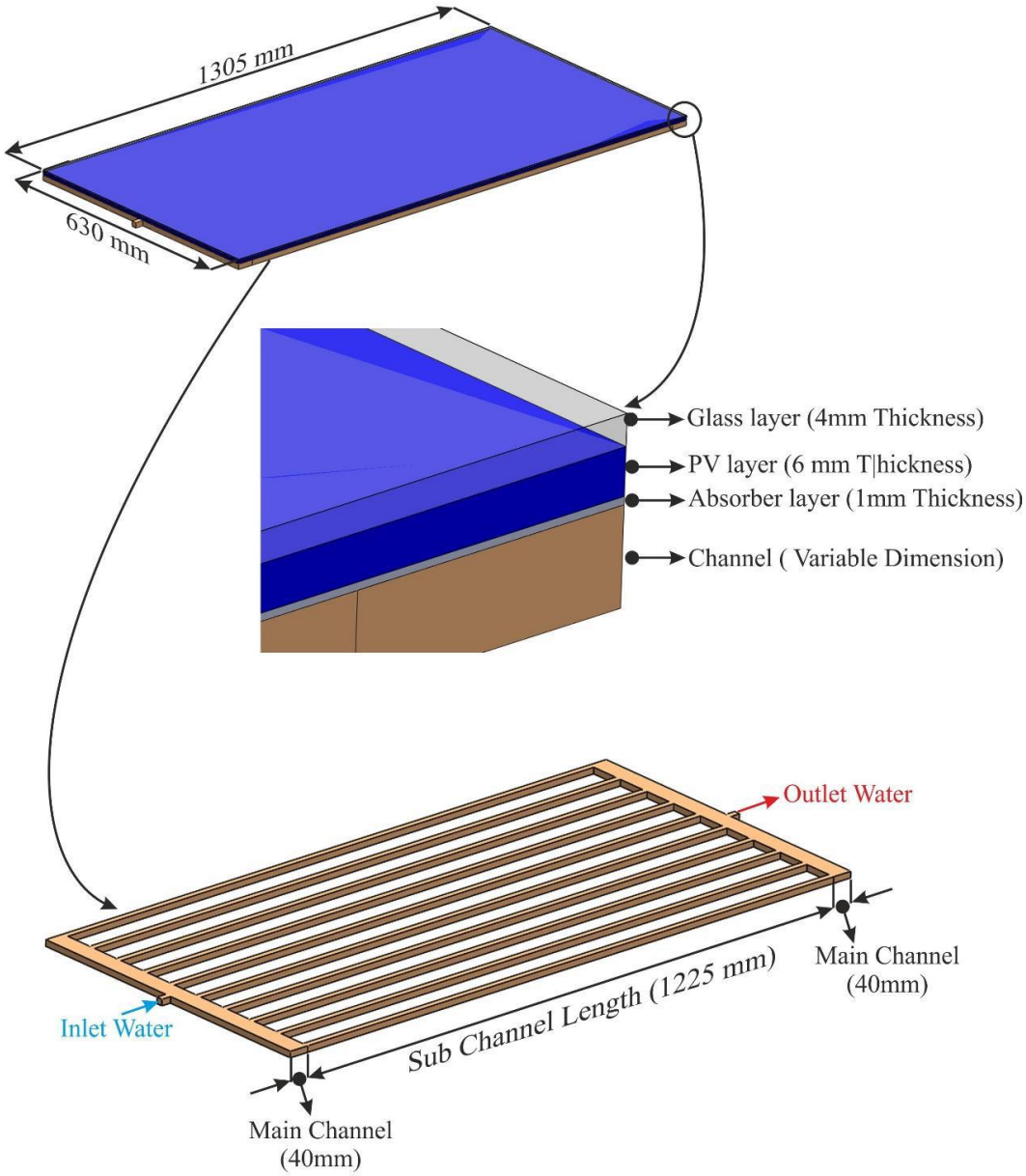

Figure 3.2. Dimension of the PVT system.

Table 3.2. Sub channels dimensions for four modules.

Cases	Sub channels Dimensions (mm)
Case 1	10×10
Case 2	12.5×12.5
Case 3	15×15
Case 4	20×20

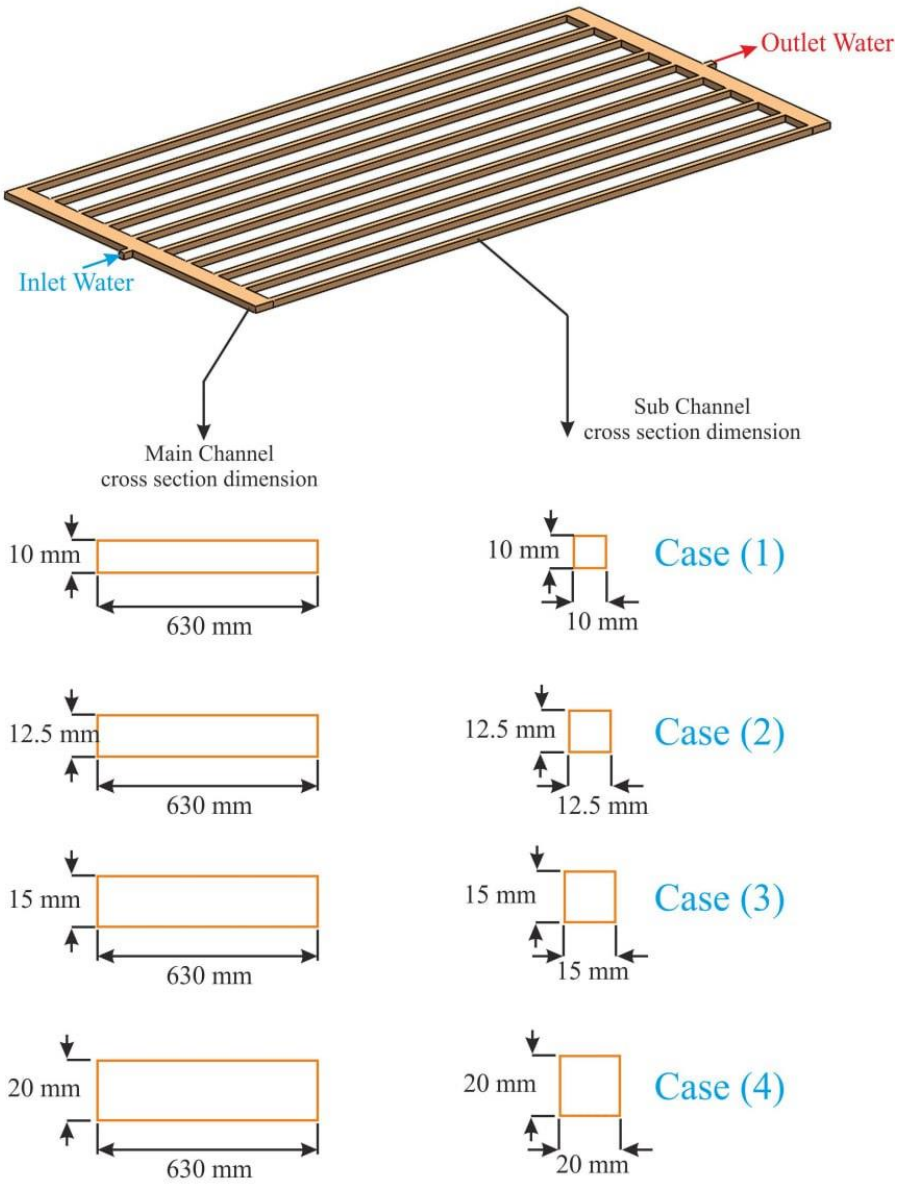

Figure 3.3. Dimension of sub channels.

3.4. MESH GENERATION

Meshing is the process of dividing a geometrical model into a finite number of elements in order to get accurate result and close to the reality. Since the mesh is generated utilizing the software Gambit 2.4.6, the meshing generation operation has an impact on the simulation's convergence, accuracy, and speed. The geometry is after that exported to the ANSYS Fluent (2021) software. In this study, the meshing utilized 3D elements. Tetrahedron meshing was applied on the PVT model to get better meshing scheme as depicted in figure 3.4.

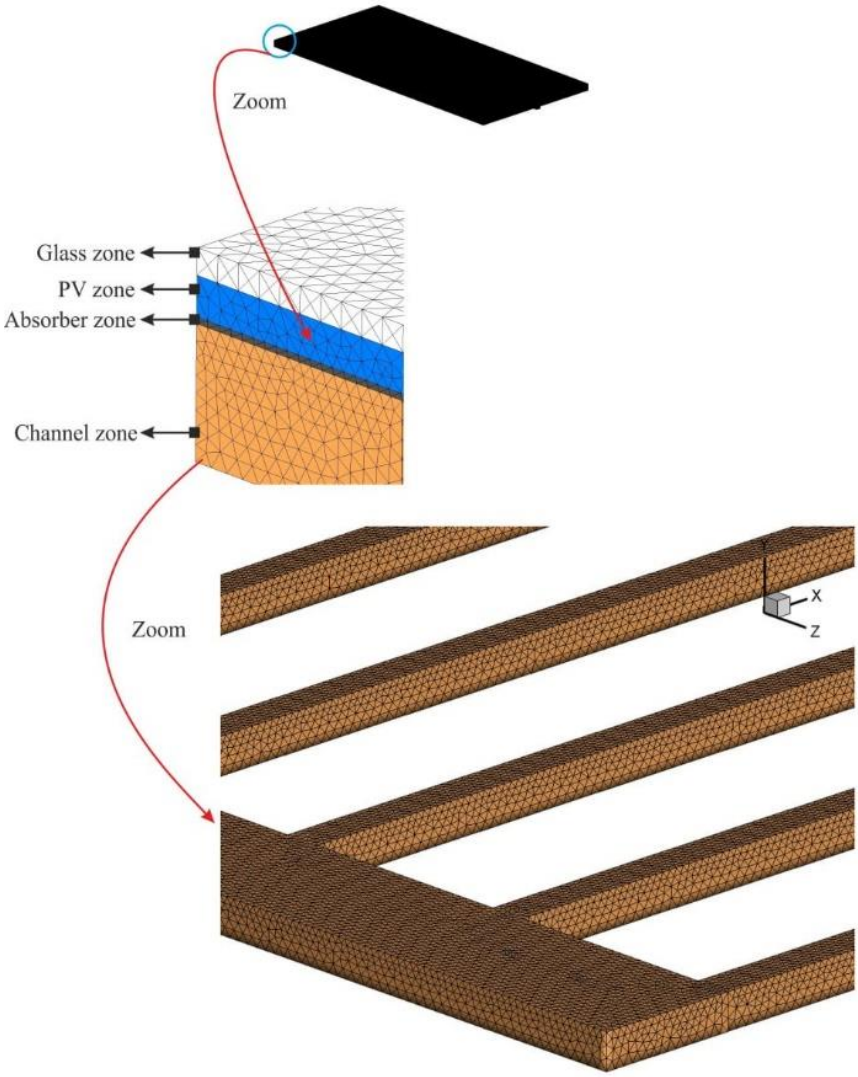

Figure 3.4. Meshing scheme for PVT system.

3.5. GRID INDEPENDENCE OF THE MODEL

ANSYS Fluent software was used to discretize the numerical model used in the study. The mesh independency test was carried out to demonstrate the accuracy of the numerical analysis. The mesh for this work was examined by modifying the parameters as well as repeating the simulation work to confirm the results' validity, and the main technique employed in this test was to increase the number of elements until it reached a point where the change in results was not noticeable. Figure 3.5 illustrates that when the number of elements increases, the average temperature of solar modules with parallel cooling channels does not change much. The mesh size (3953596) for the model is the optimal size to use for the simulation calculation process and it takes less time to finish the process, as revealed in table 3.3.

Table 3.3. Mesh independence test.

Elements	The average temperature on PV panel
2506679	36.12
3009865	37.56
3953596	38.21
4904192	38.24
6490213	38.25

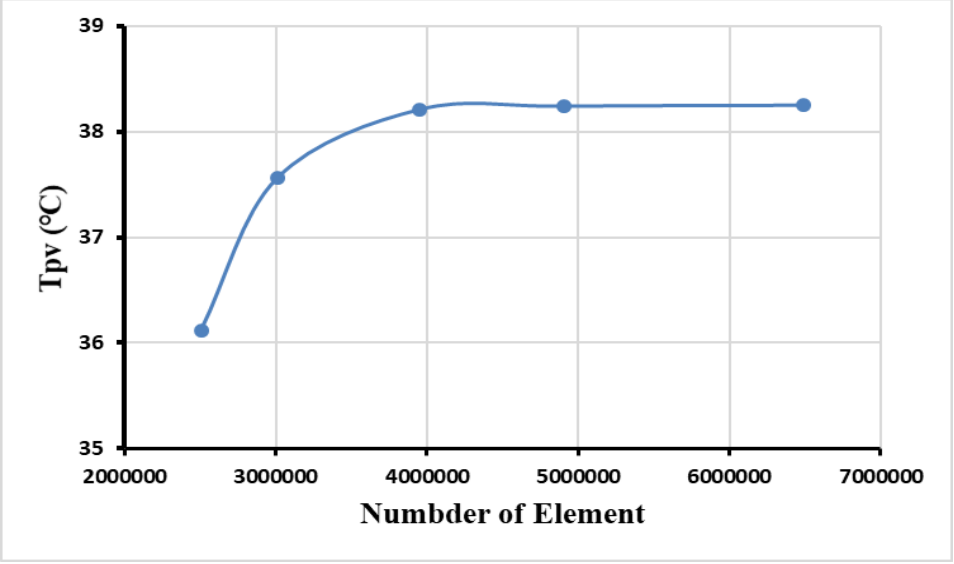

Figure 3.5. Mesh independent test of the photovoltaic modules' average temperature.

3.6. MODEL VALIDATION

The average temperature of PV modules with parallel cooling channels determined from numerical results is compared with those estimated in [41] to evaluate the numerical model built in this simulation with the use of ANSYS fluent software. Based on the geometry parameters (10 sub-channels and I inlet outlet configuration) and governing equations, as illustrated in figure 3.6, under the same identical boundary conditions in present study, the average temperatures of solar modules are validated. Table 3.4 compares the simulation study being presented and the prior study [41], with the greatest percentage error being (3.18%).

Table 3.4. Comparision between the current numerical results and prior study.

Re	T_ PV simulation	T_ PV paper
920	42.32	43
1200	40.94	40
1520	39.38	38
1600	38.82	37
1850	37.76	36
2275	36.72	35

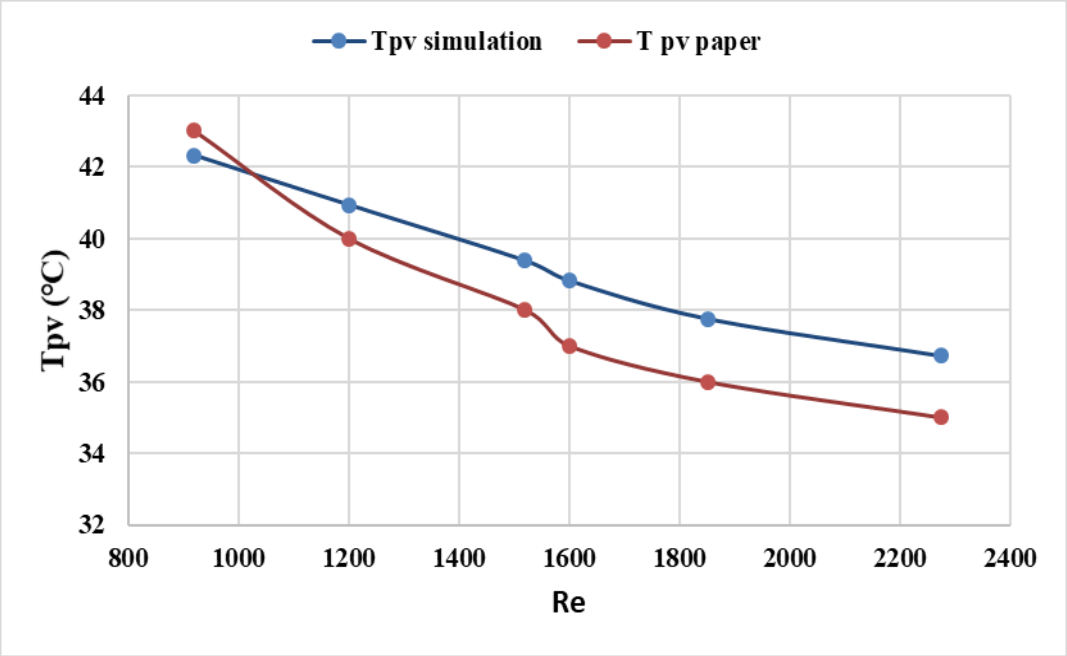

Figure 3.6. Comparison between the current numerical results and prior study.

PART 4

RESULTS AND DISCUSSION

In this chapter, the findings of the numerical analyses in the PVT water collector were discussed, analyses were done to demonstrate the effects of various sub channel dimensions on the temperature of the photovoltaic module, temperature distribution, pressure drop, velocity distribution. The change in the dimensions of the sub channels leads to a change in the liquid flow characteristics in the channels and thus affects the cooling of the solar panel module. Four dimensions are selected to take out the effect of dimensions on the PVT collector.

4.1. EFFECT OF THE SUB CHANNEL DIMENSION ON THE TEMPERATURE DISTRIBUTION OF THE PV PANEL

Figure 4.1 to 4.12 illustrates the impact of different sub channel sizes (10*10), (12.5*12.5), (15*15), and (20*20) mm in a PVT collector on the photovoltaic module surface temperatures and temperature distributions in the cooling channels for Reynold numbers Re (920,1200,1520,1600,1850 and 2275). The numerical analyses demonstrate that the temperature of the solar cell decreases as the sub channels dimension increase, therefore the temperature is lower in the large diameter compared to the smaller diameters. As a result, the case of 20*20 mm has a lower PV temperature and a more even distribution because increasing the surface area in the vast diameter improves the contact between the water sub channels and the PV panel.

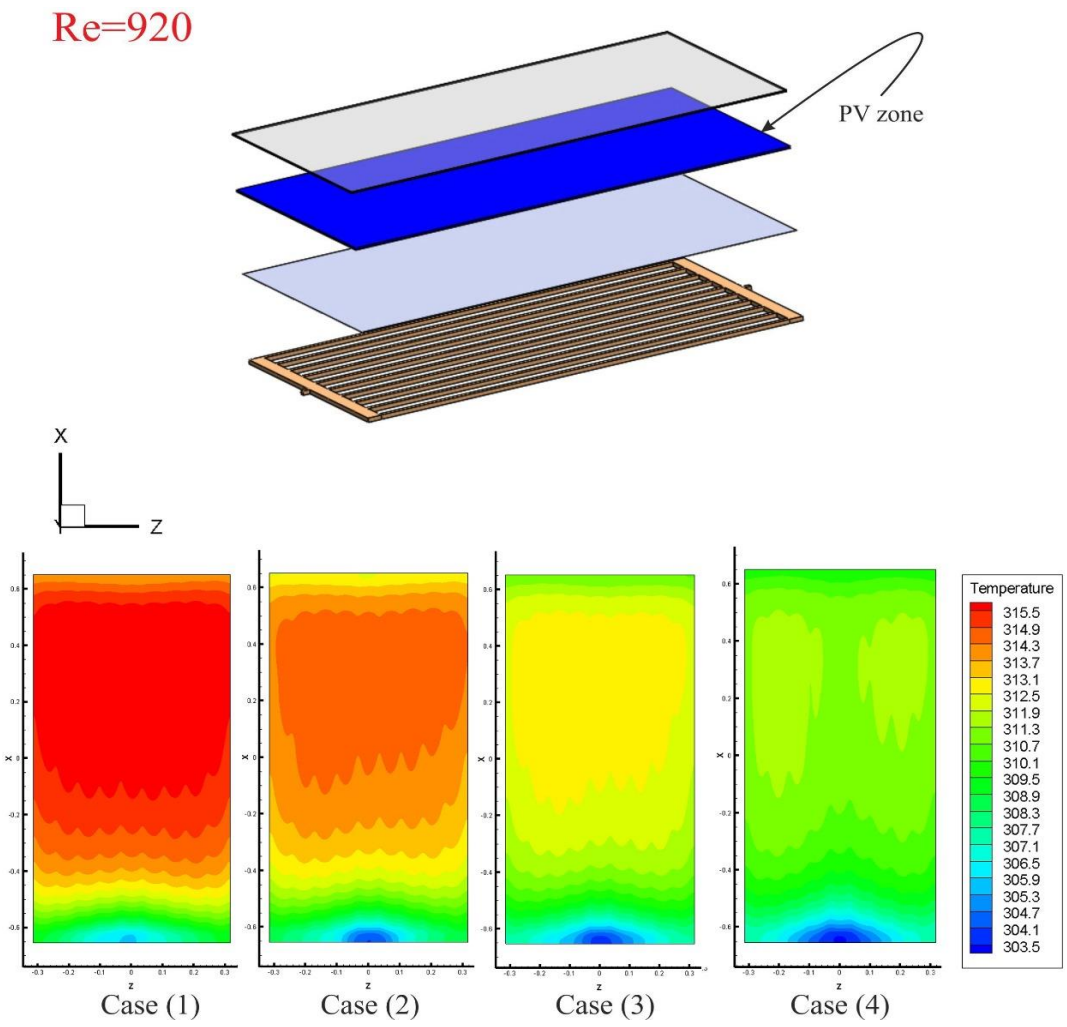

Figure 4.1 Average temperature photovoltaic module at Re 920.

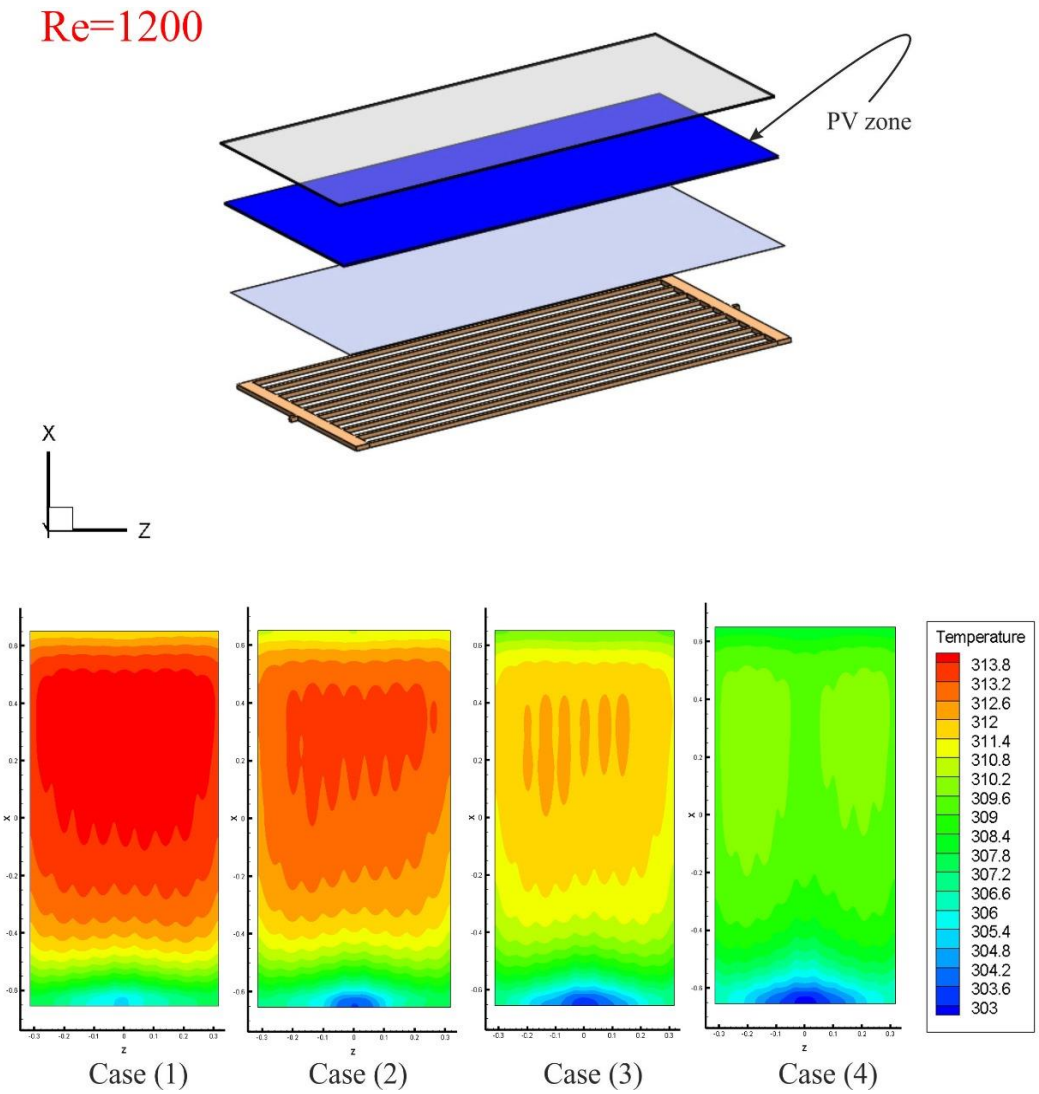

Figure 4.2. Average temperature photovoltaic module at Re 1200.

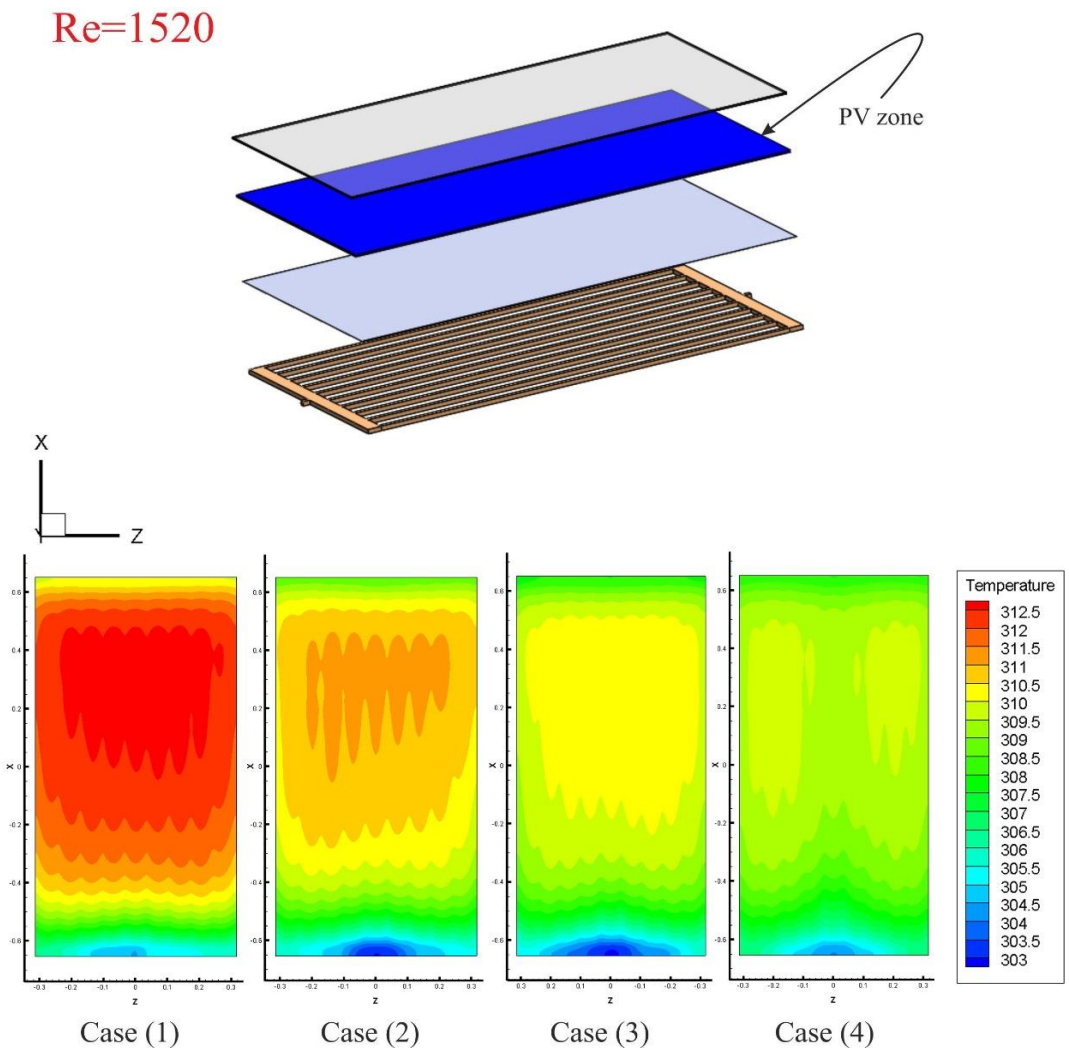

Figure 4.3. Average temperature photovoltaic module at Re 1520.

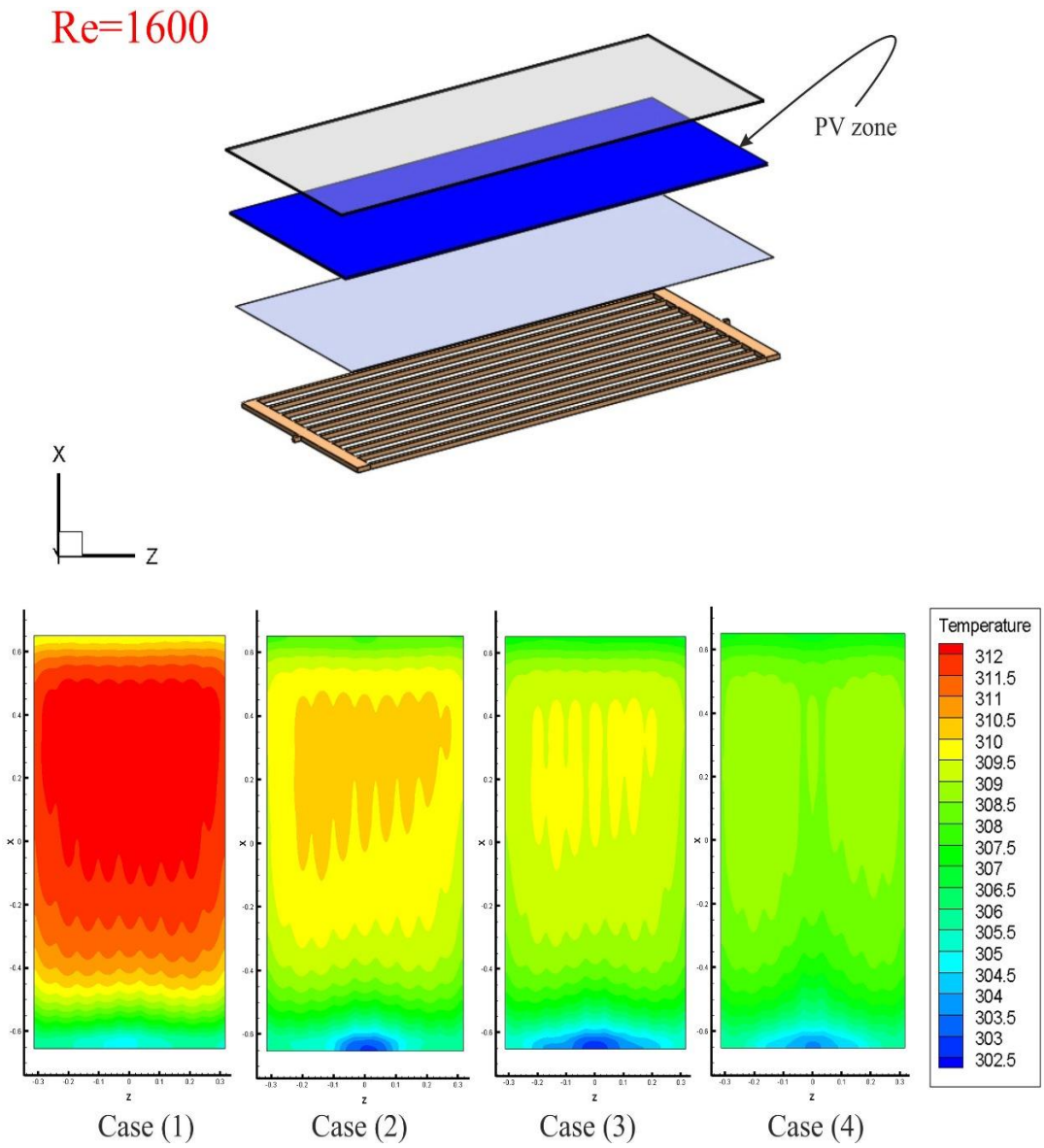

Figure 4.4. Average temperature photovoltaic module at Re 1600.

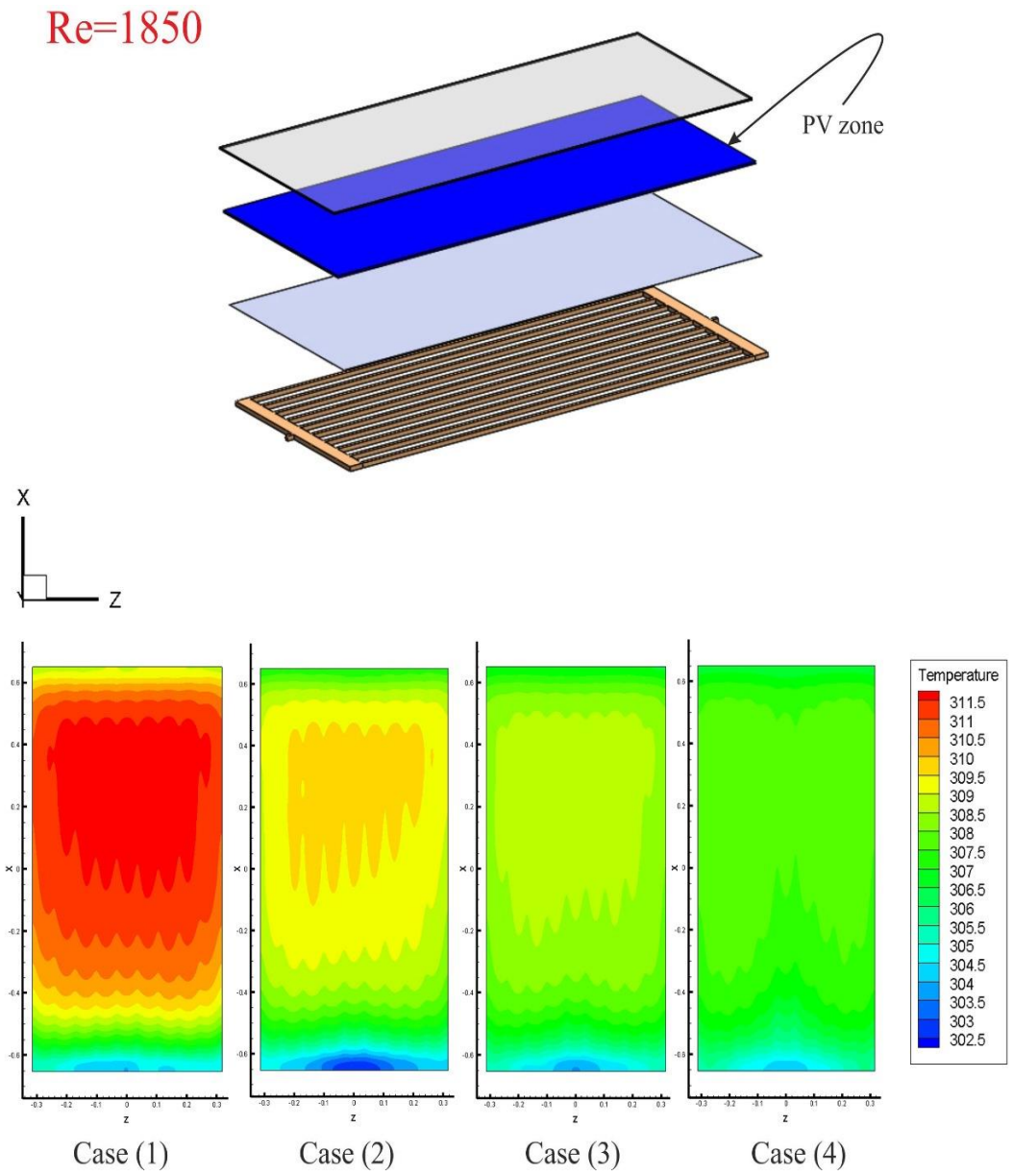

Figure 4.5. Average temperature photovoltaic module at Re 1850.

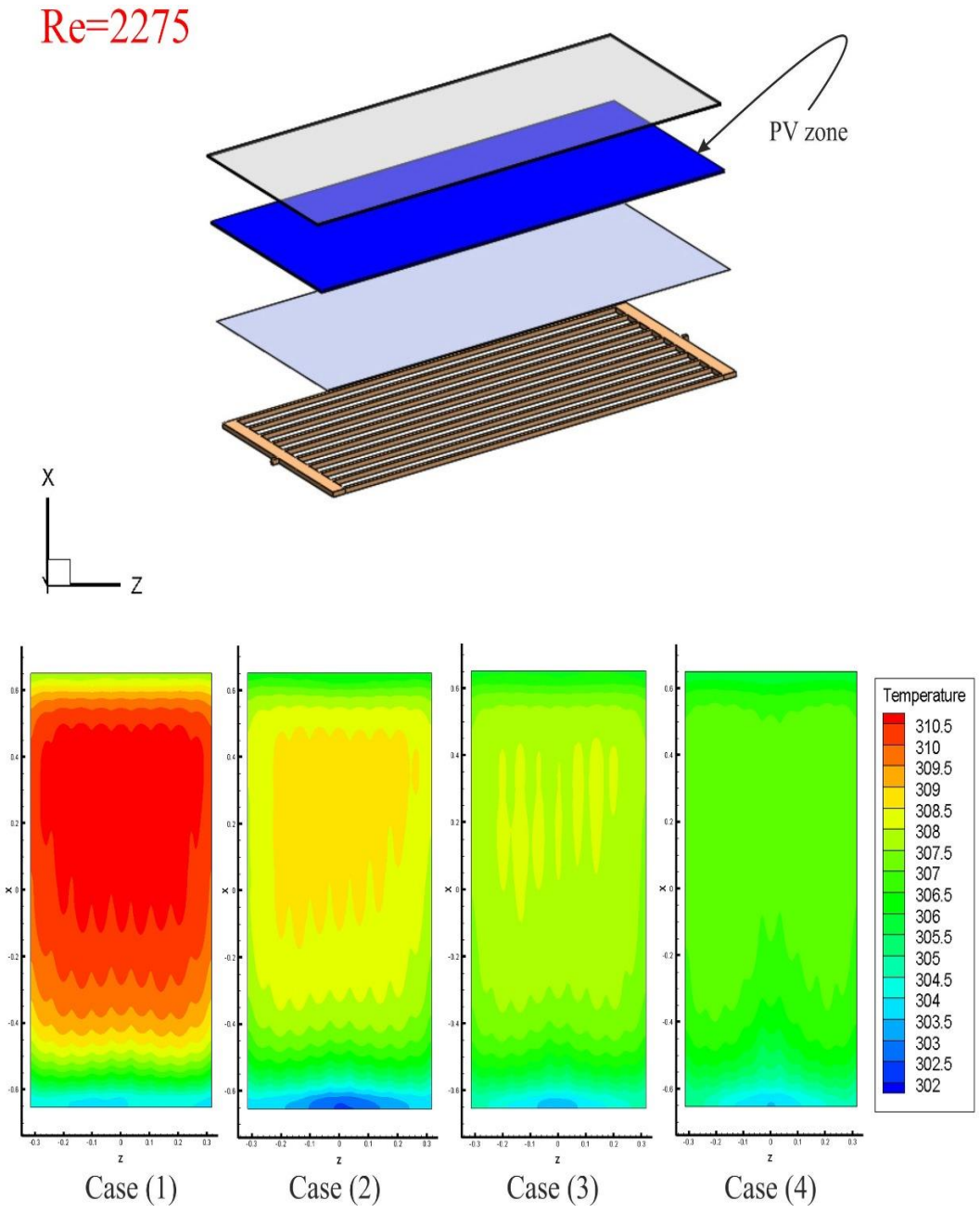

Figure 4.6. Average temperature photovoltaic module at Re 2275.

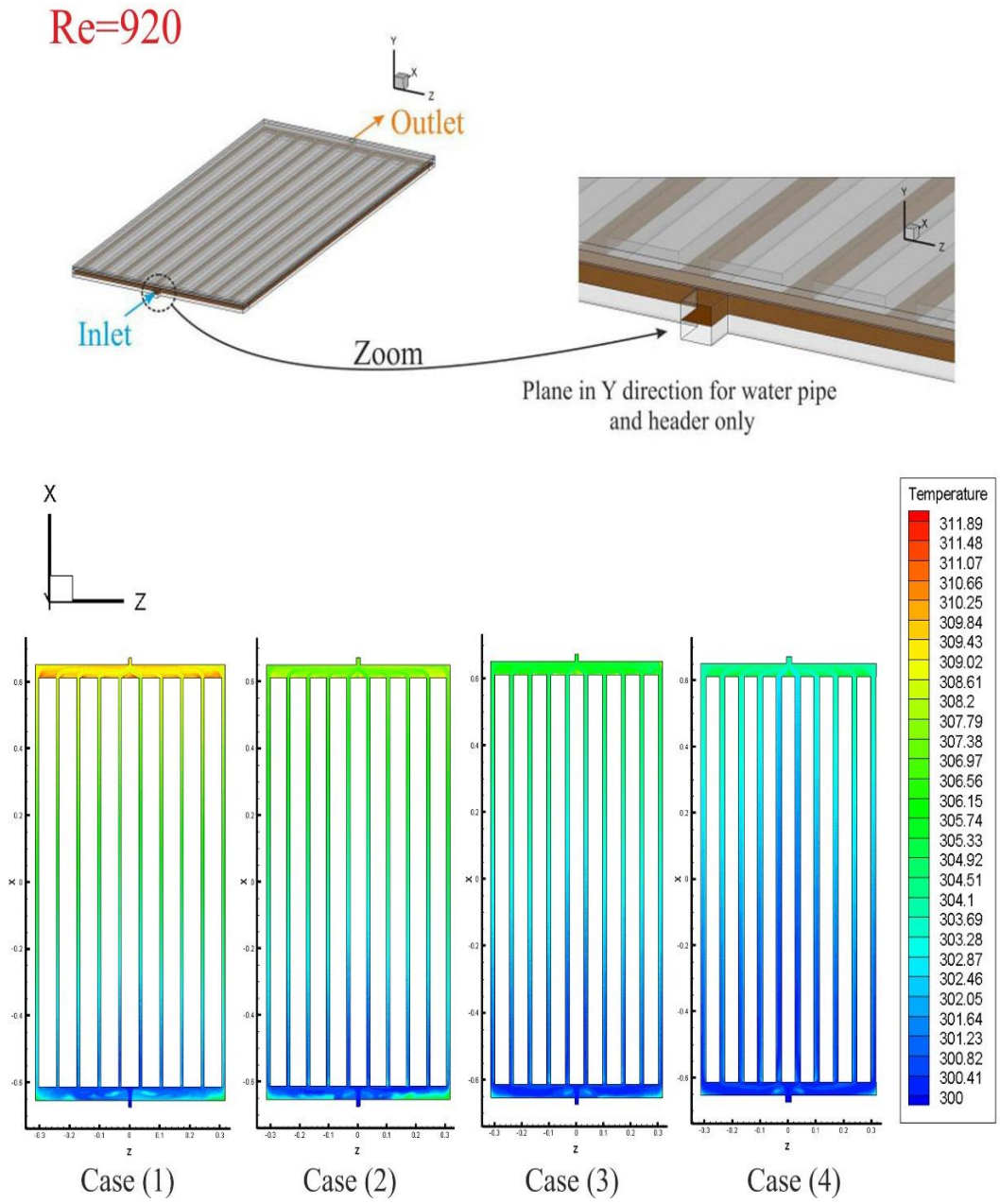

Figure 4.7. Temperature distributions in cooling channels for Re 920.

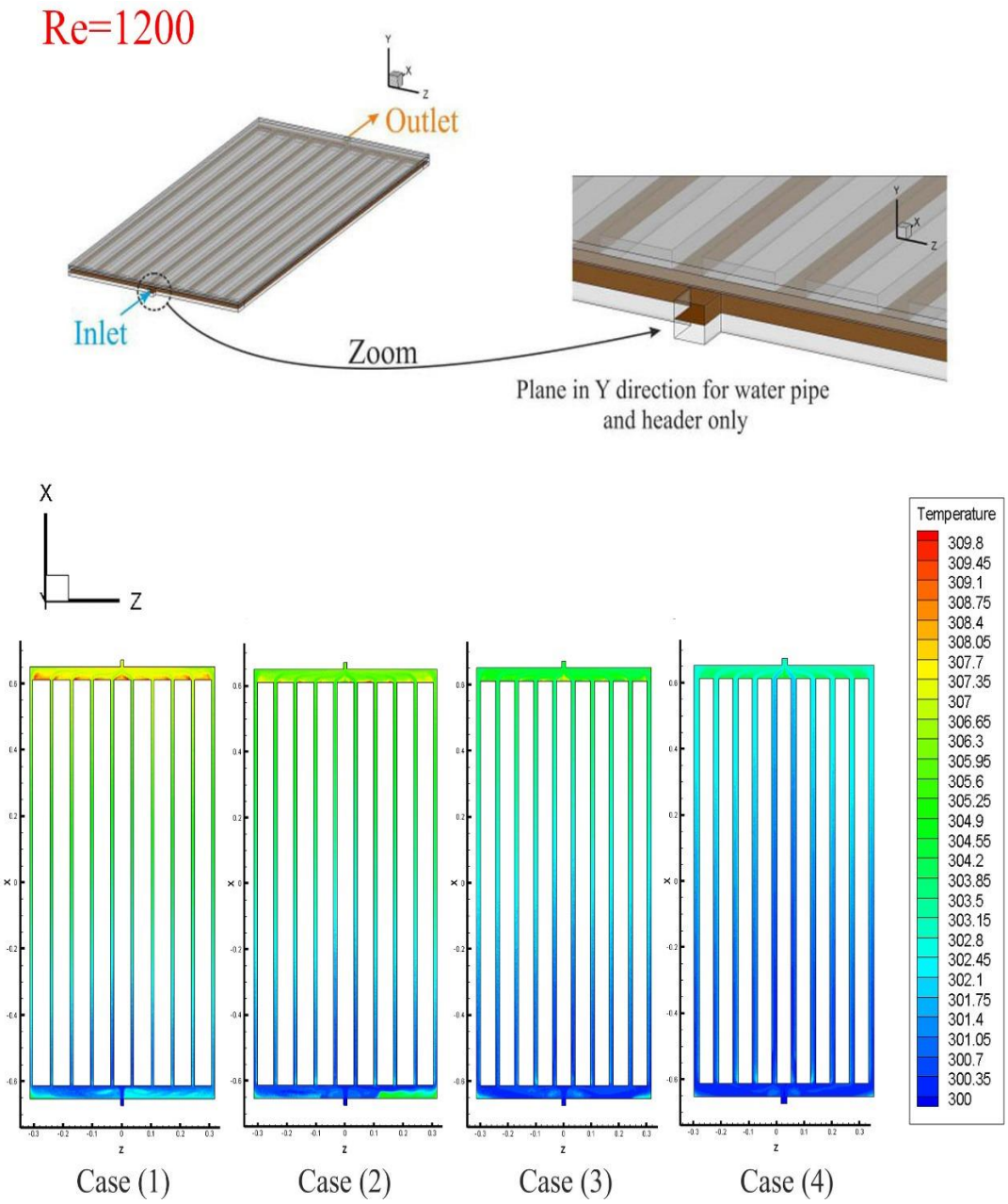

Figure 4.8. Temperature distributions in cooling channels for Re 1200.

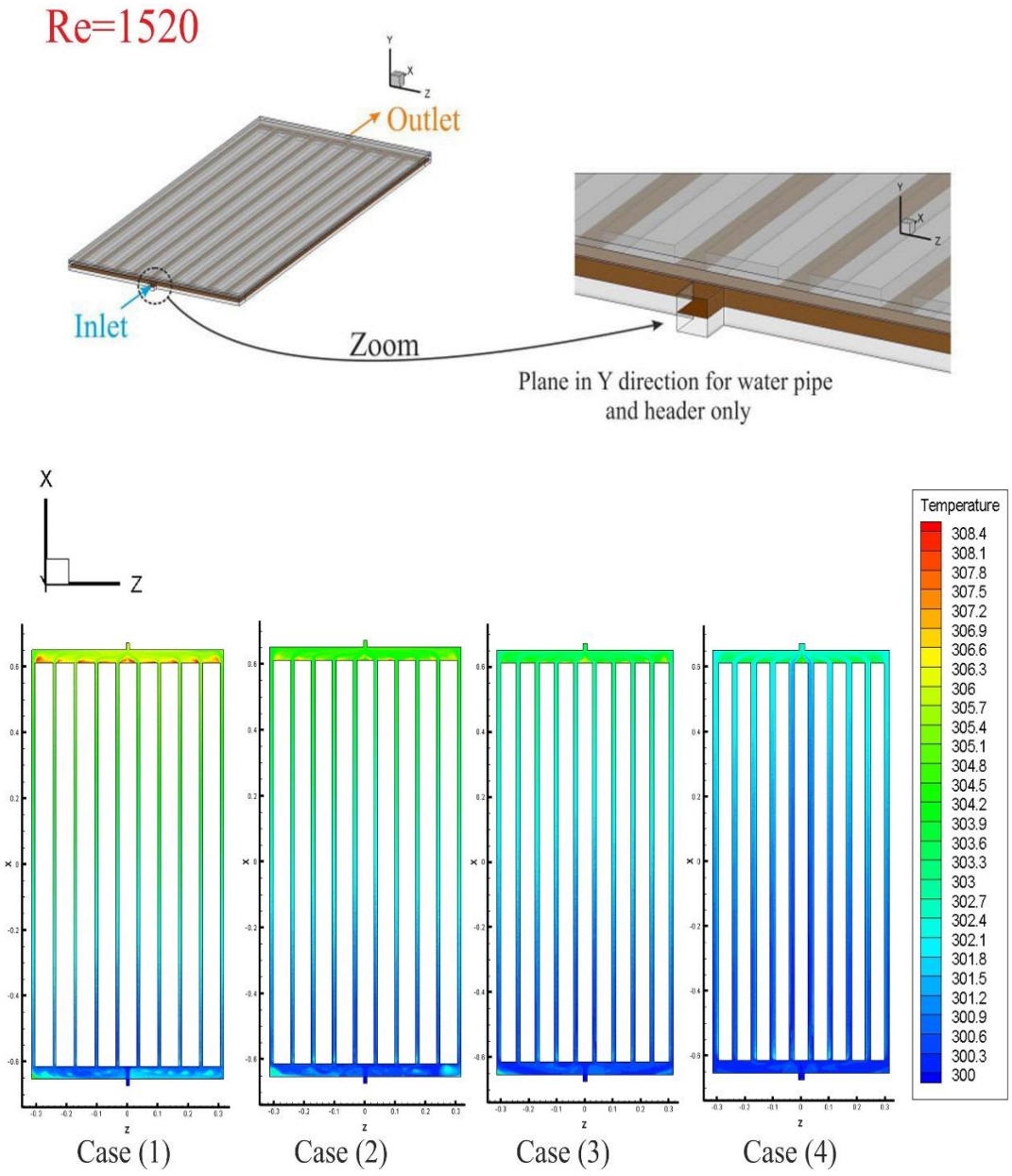

Figure 4.9 . Temperature distributions in cooling channels for Re 1520.

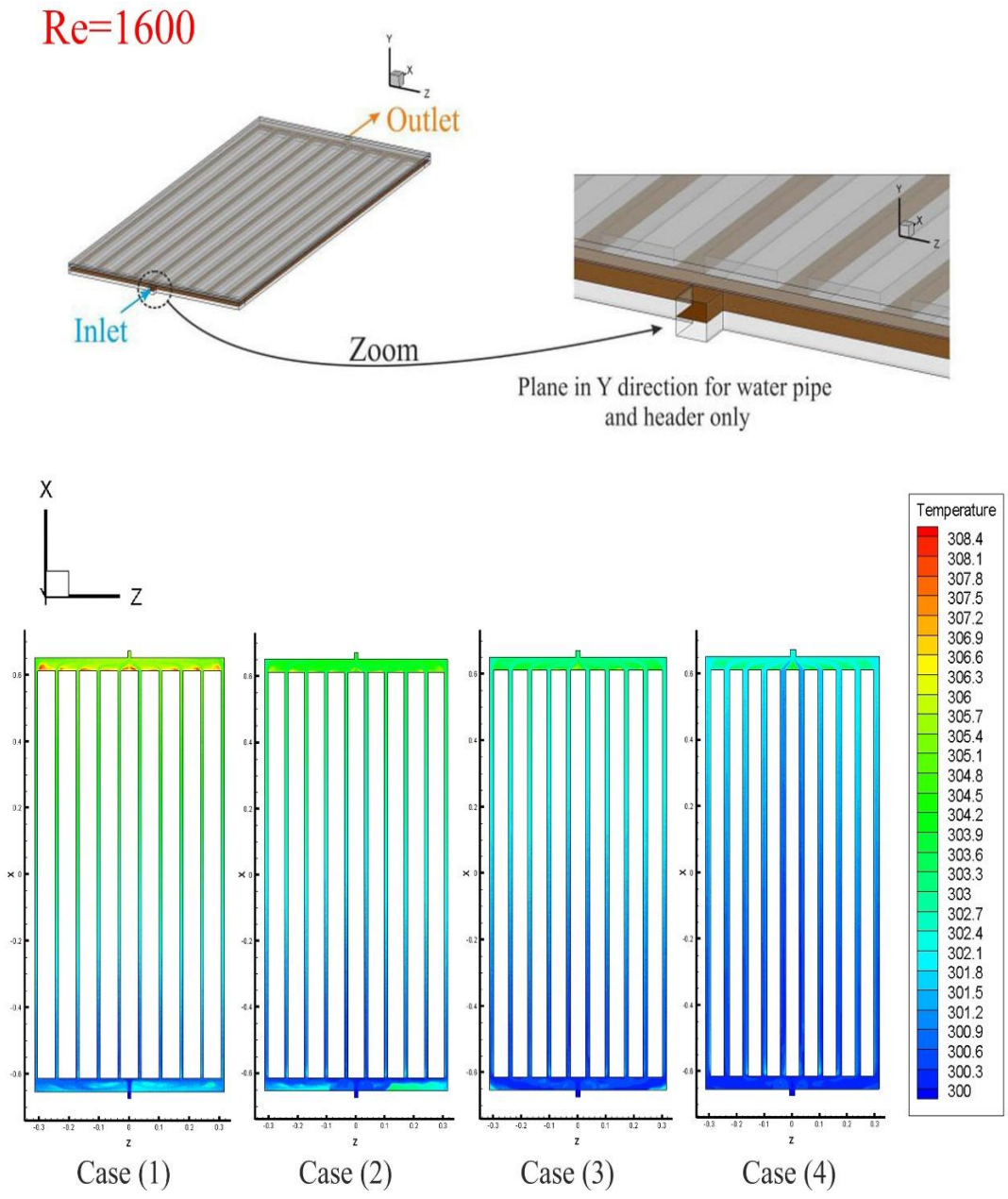

Figure 4.10. Temperature distributions in cooling channels for Re 1600.

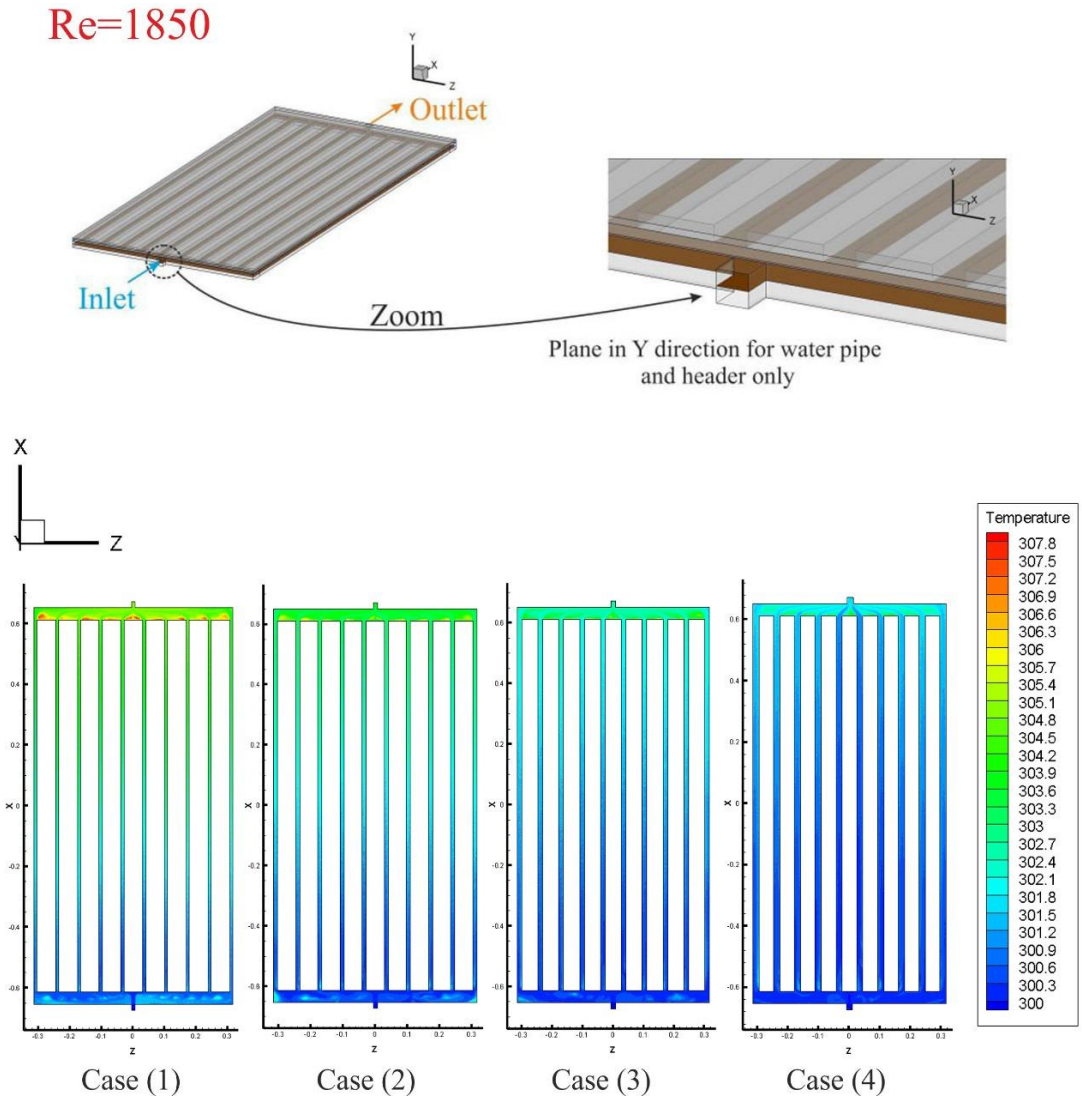

Figure 4.11. Temperature distributions in the cooling channels for Re 1850.

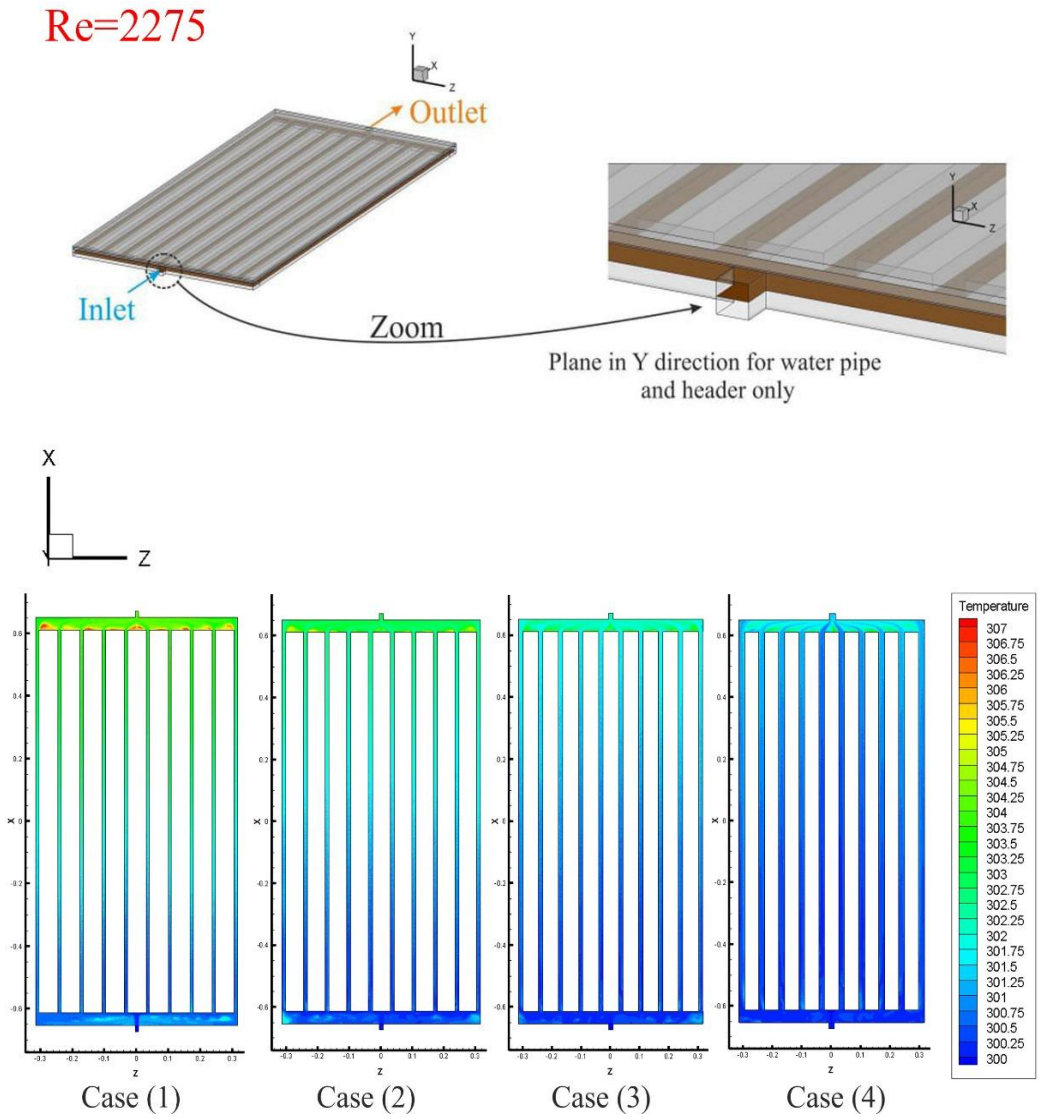

Figure 4.12. Temperature distributions in cooling channels for Re 2275.

Figure 4.13 manifests the average temperature of PV module in different cases of sub channels' dimensions. From the curves, we find that in case of 10*10, the average temperature of the module was 41.45 °C when Re=920 and dropped to 36.43 °C when Re=2275. When Re was increased from 920 to 2275, The module's average temperature decreased from 40.1 °C to 34.58 °C in the second case, which has a diameter of 12.5*12.5 sub channel. For the third case, which is the dimension of 15*15 sub channel, the module's average temperature varied from 38.53 °C downward to 33.61 °C when Re was increased from 920 to 2275.The module average temperature in the last case 20*20 changed from 37.28 °C to 32.63 °C in the

same range of Re. This occurs as a result of the increase in contact area between the water sub channels and the solar panel.

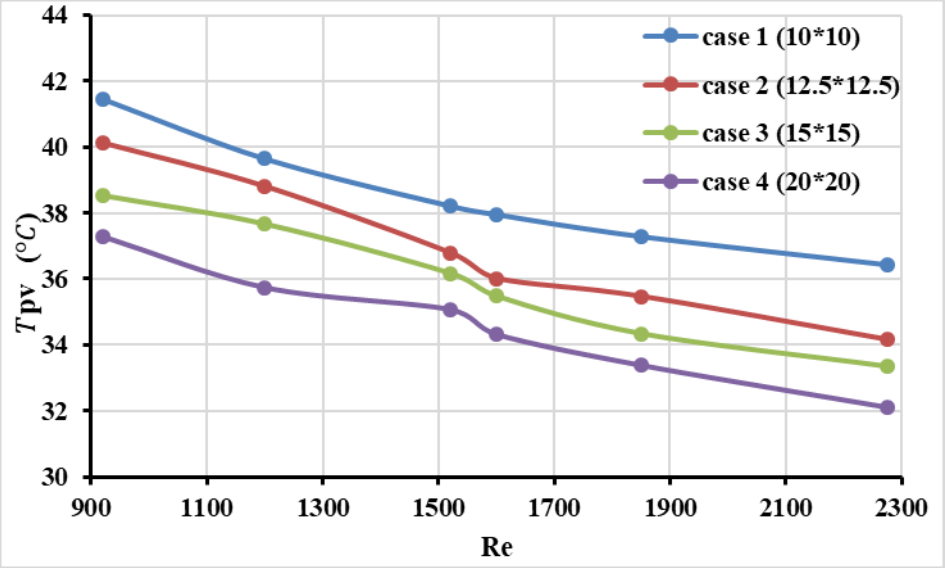

Figure 4.13. The photovoltaic module's average temperature in four cases with various Reynolds values.

Also, from average temperatures curves we can take out that the average temperature of the photovoltaic module decreases with the increase of Reynolds number (Re) in the four cases of the study. The average temperatures for Re=1520 were 38.2 °C, 36.78 °C, 36.17 °C and 35.07 °C, respectively. When Re=2275 in the present study, those values were 36.43°C ,34.16 °C, 33.61 °C and 32.63 °C, respectively. Figure 4.14 presents that the large dimension's sub channels have the low average temperature.

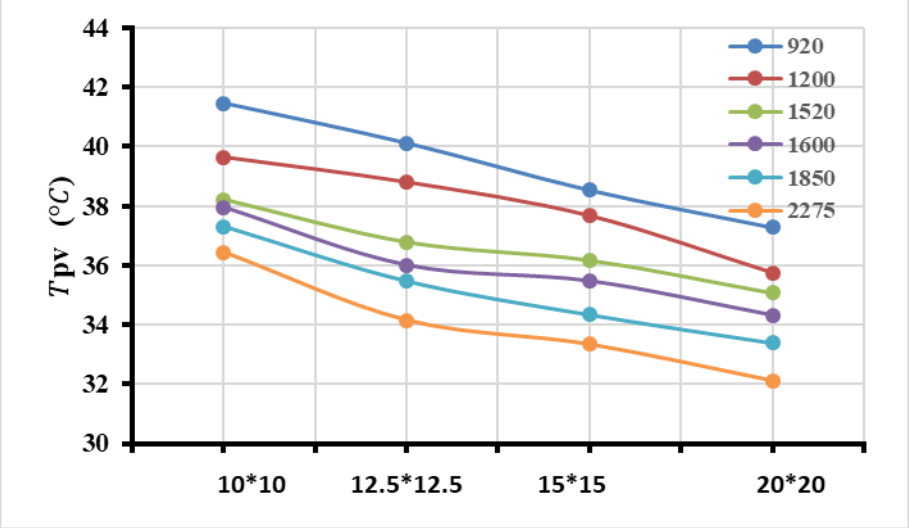

Figure 4.14. The change in the average PV temperature with the change in Re number.

4.2. EFFECT OF THE SUB CHANNEL DIMENSION ON THE VELOCITY DISTRIBUTION IN CHANNELS

The distributions of the velocity of the parallel channels of cooling with the four cases of dimensions (10*10), (12.5*12.5), (15*15), and (20*20) mm with different Reynold numbers Re (920,1200,1520,1600,1850 and 2275) are evinced in Figures 4.15 to 4.20. The gradient of the velocity distribution in the four-dimensional cases elucidates that the sub channels' diameters increase, and the flow velocity in all sub channel eventually decreases. Additionally, the main channel's flow velocity is noticeably greater than the sub channels. The flow is little in the fourth case (20*20) mm because of the large dimension which leads to less flow resistance, while it is more in the cases of the smallest dimensions. As for the sub-channels, the velocity gradient is almost constant, due to the distribution of the liquid flowing through the sub-channels. Since the Reynolds number and flow velocity are directly proportional, it is noted that when the Reynolds number increases, the velocity also increases.

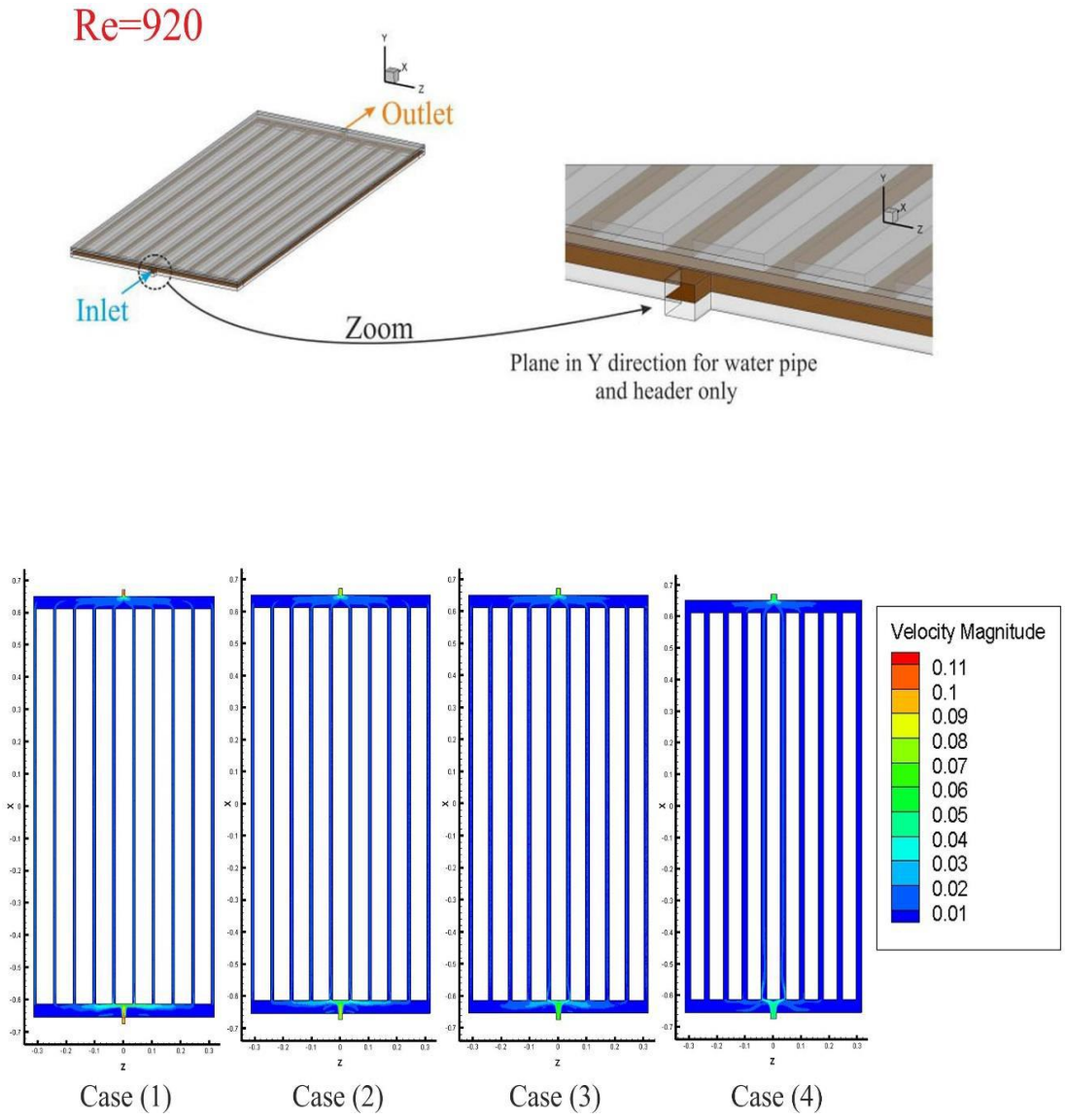

Figure 4.15. Distributions of velocity in cooling channels for Re 920.

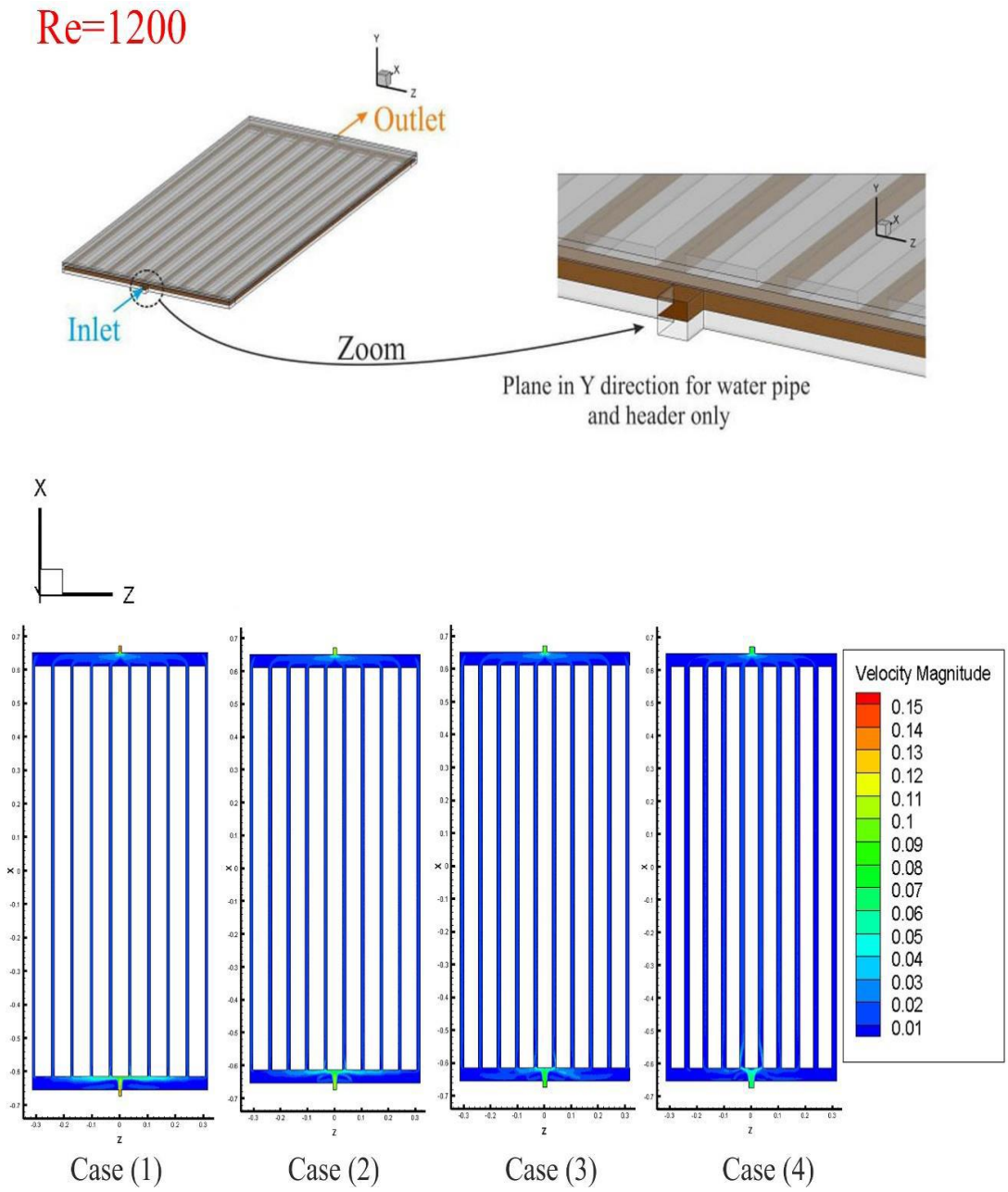

Figure 4.16. Distributions of velocity in cooling channels for Re 1200.

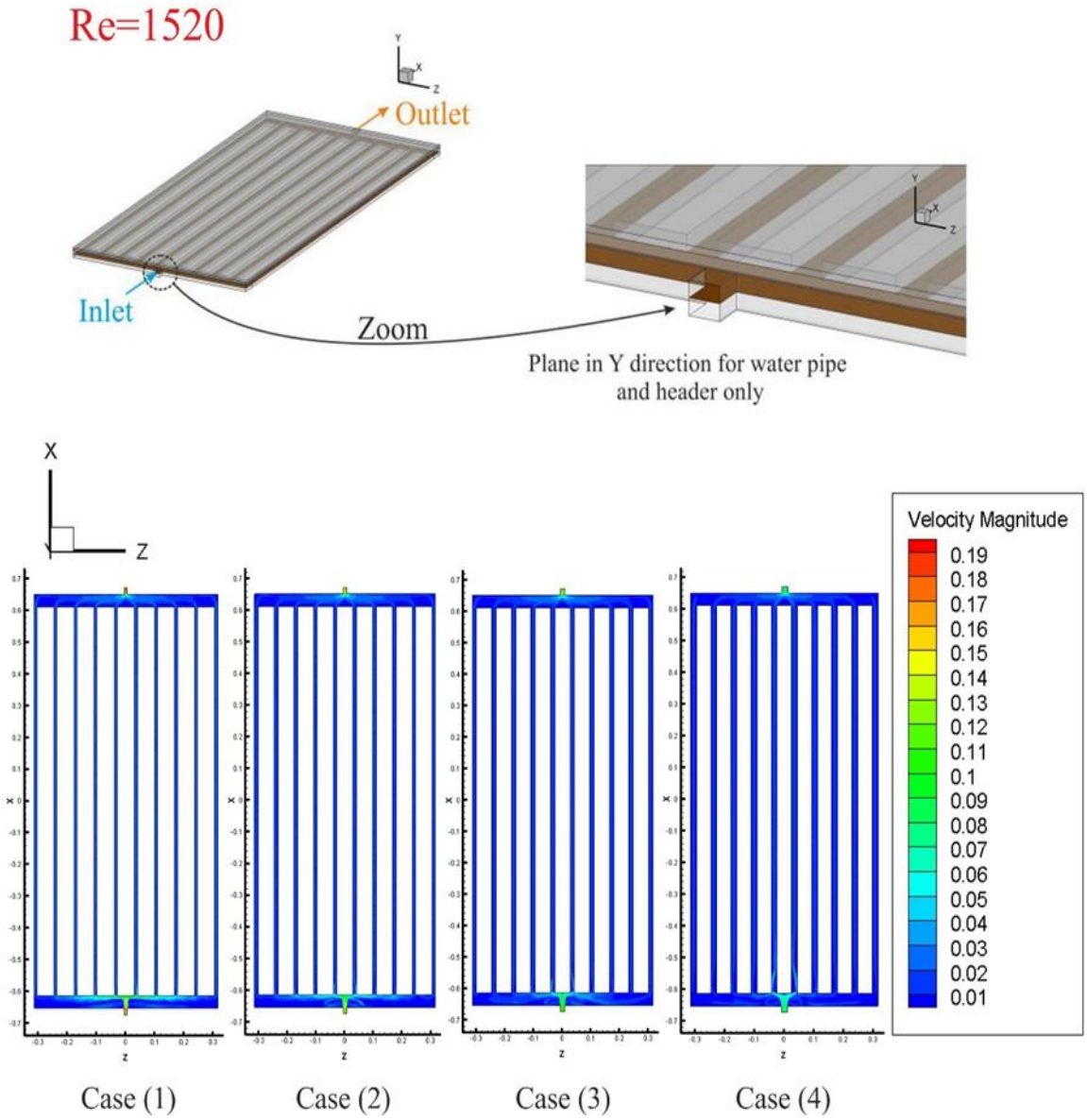

Figure 4.17. Distributions of velocity in cooling channels for Re 1520.

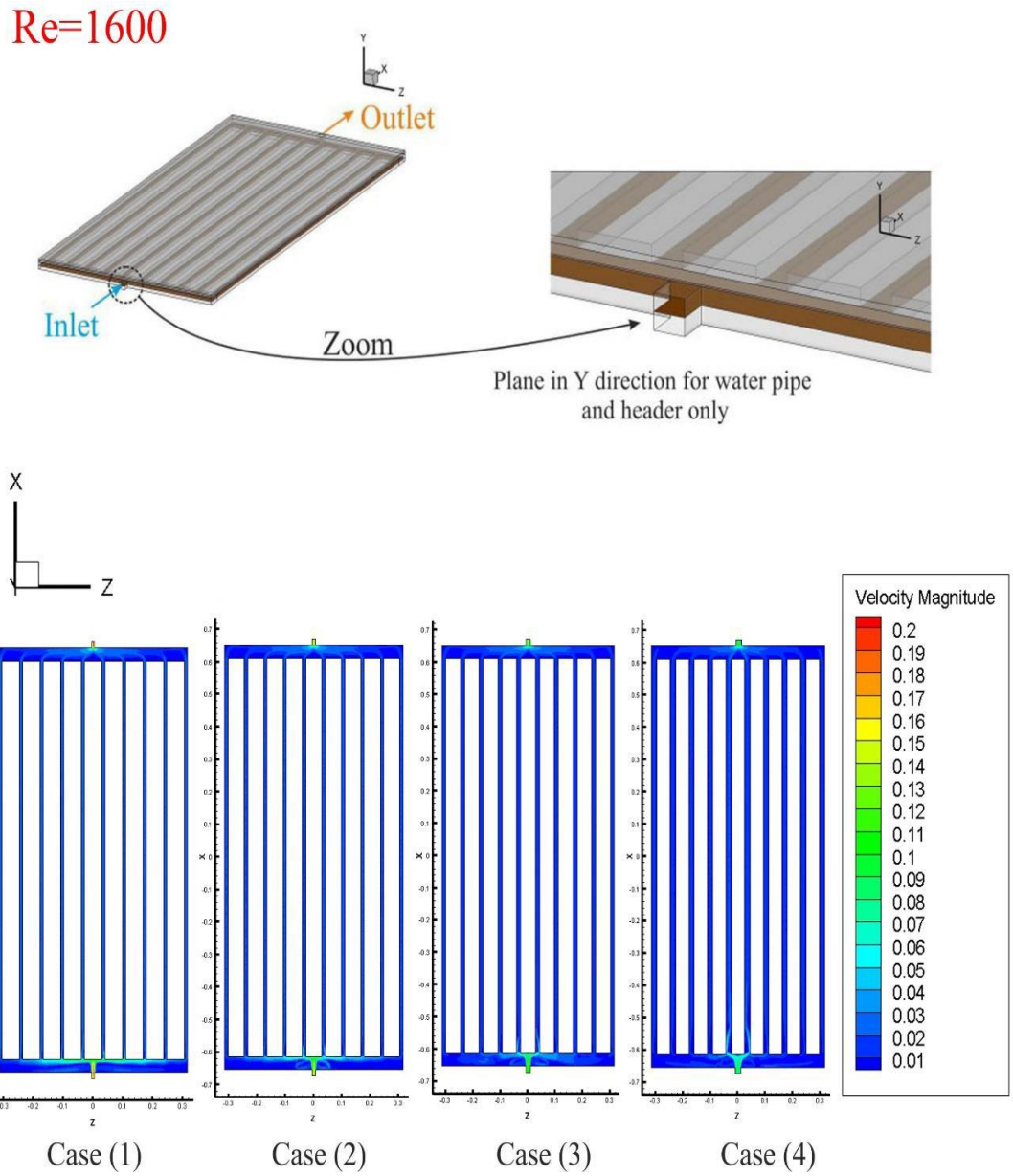

Figure 4.18. Distributions of velocity in cooling channels for Re 1600.

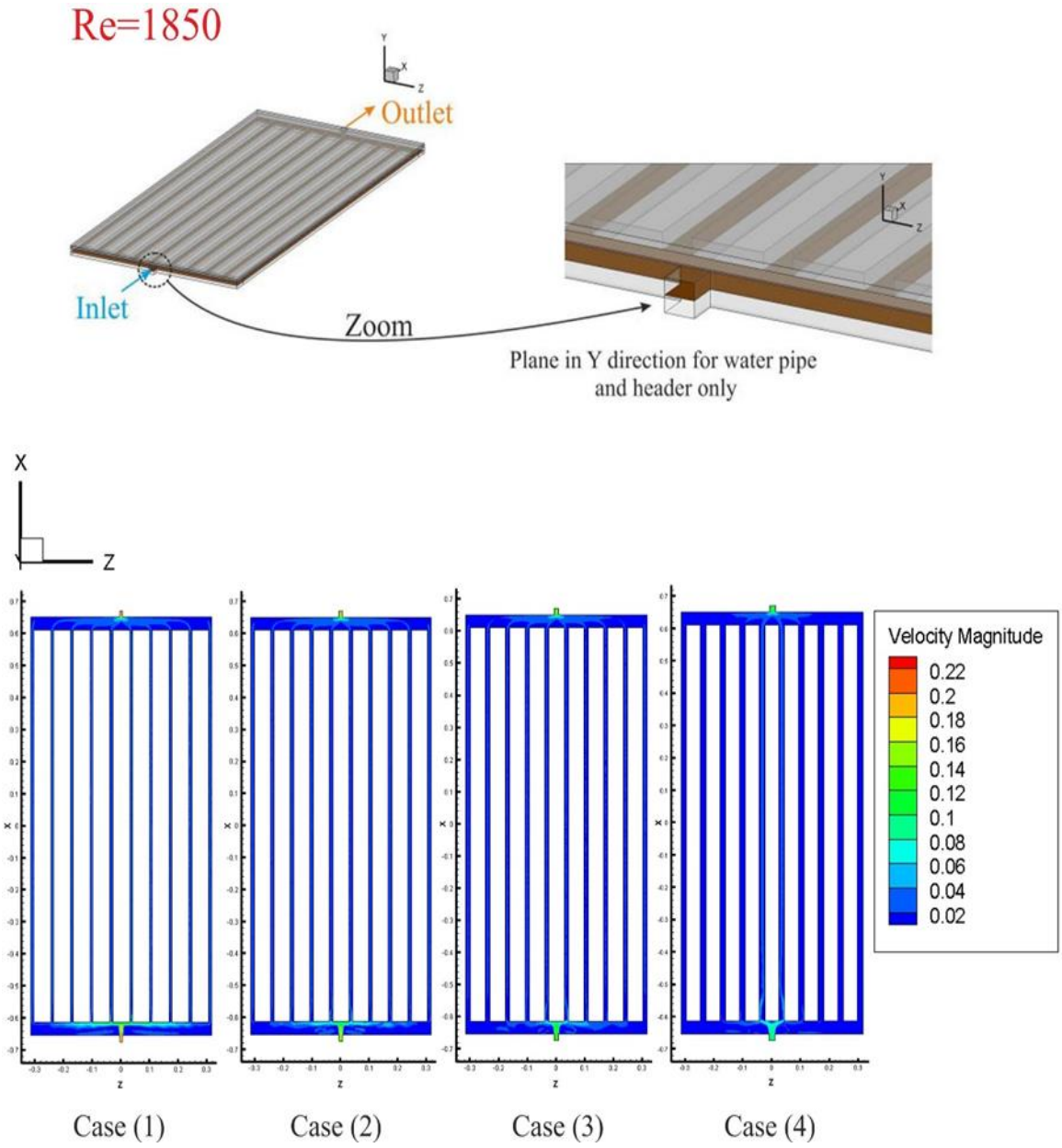

Figure 4.19. Distributions of velocity in cooling channels for Re 1850.

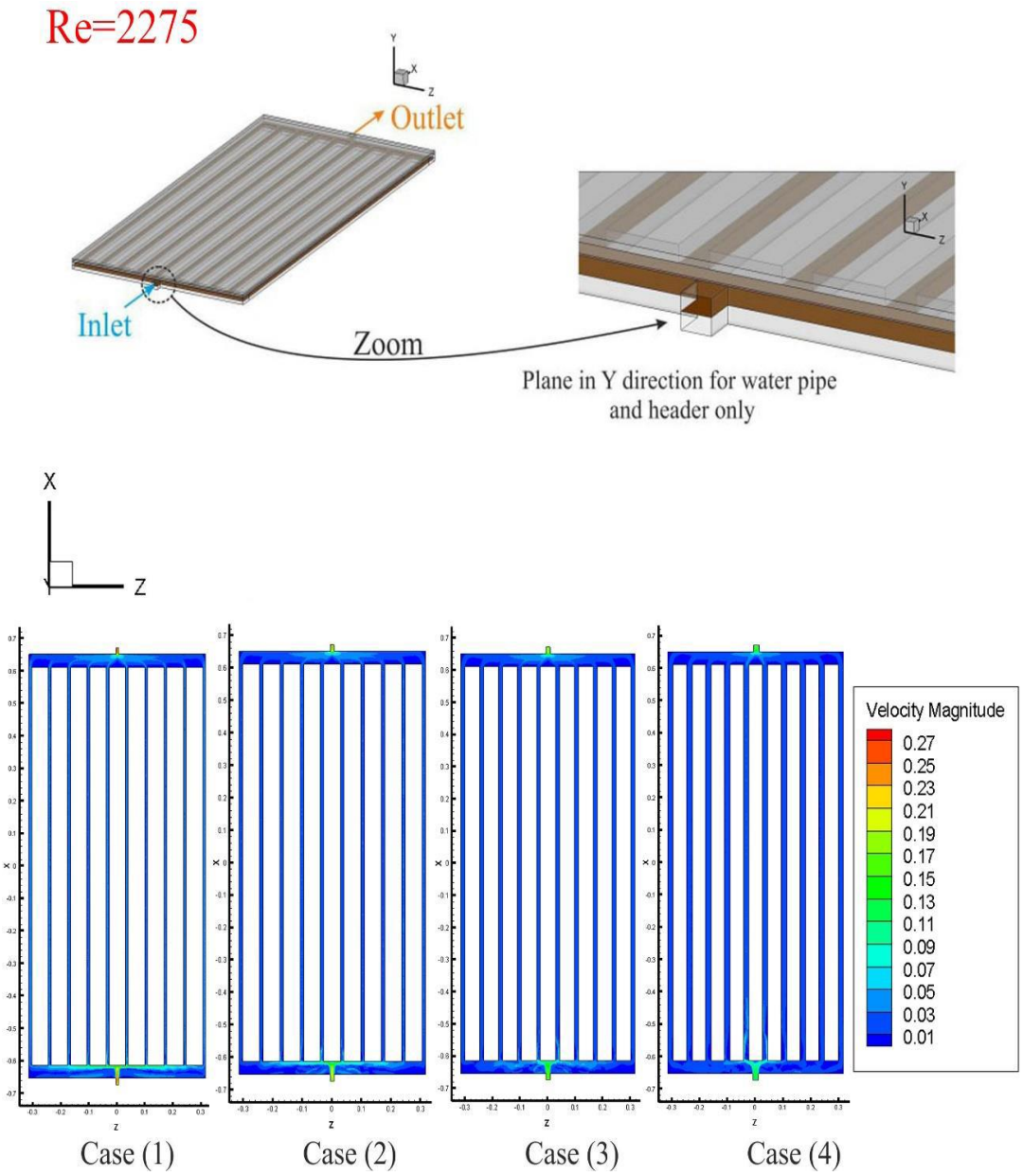

Figure 4.20. Distributions of velocity in cooling channels for Re 2275.

4.3. EFFECT OF THE SUB CHANNEL DIMENSION UPON THE PRESSURE DROP THROUGH THE COOLING CHANNELS

Figures 4.21 to 4.26 display the distribution of the pressure in the main and sub-cooling channels for the four cases of sub channels' dimensions (10*10), (12.5*12.5), (15*15), and (20*20) mm for different values of Reynolds number (Re) (920,1200,1520,1600,1850 and 2275). Where, it is shown that with the increase in the sub channels section size, the pressure drop decreases, due to the fluid velocity

decrease, and thus the on-way decreases in frictional resistance with the increase in the dimensions of the flow section.

Re=920

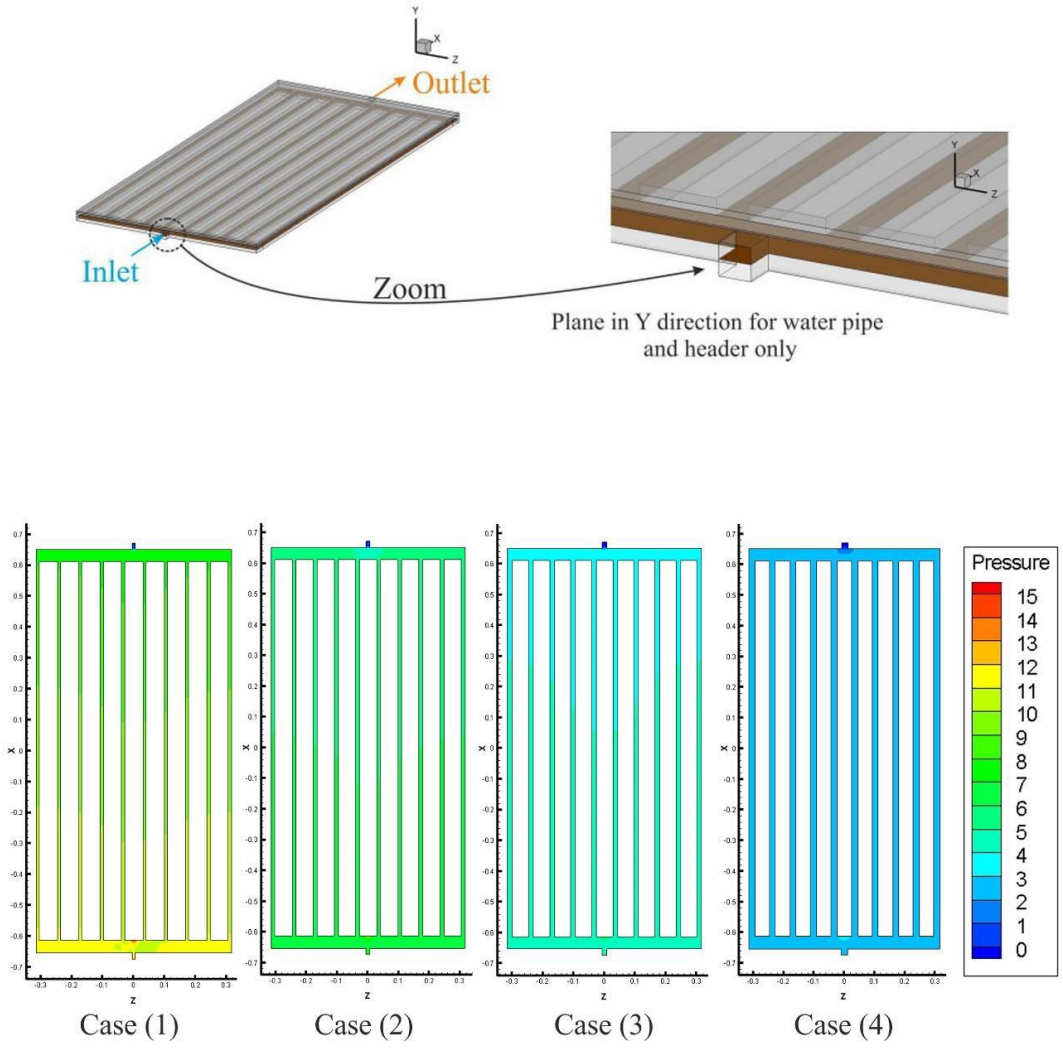

Figure 4.21. Distributions of pressure in cooling channels for Re 920.

Re=1200

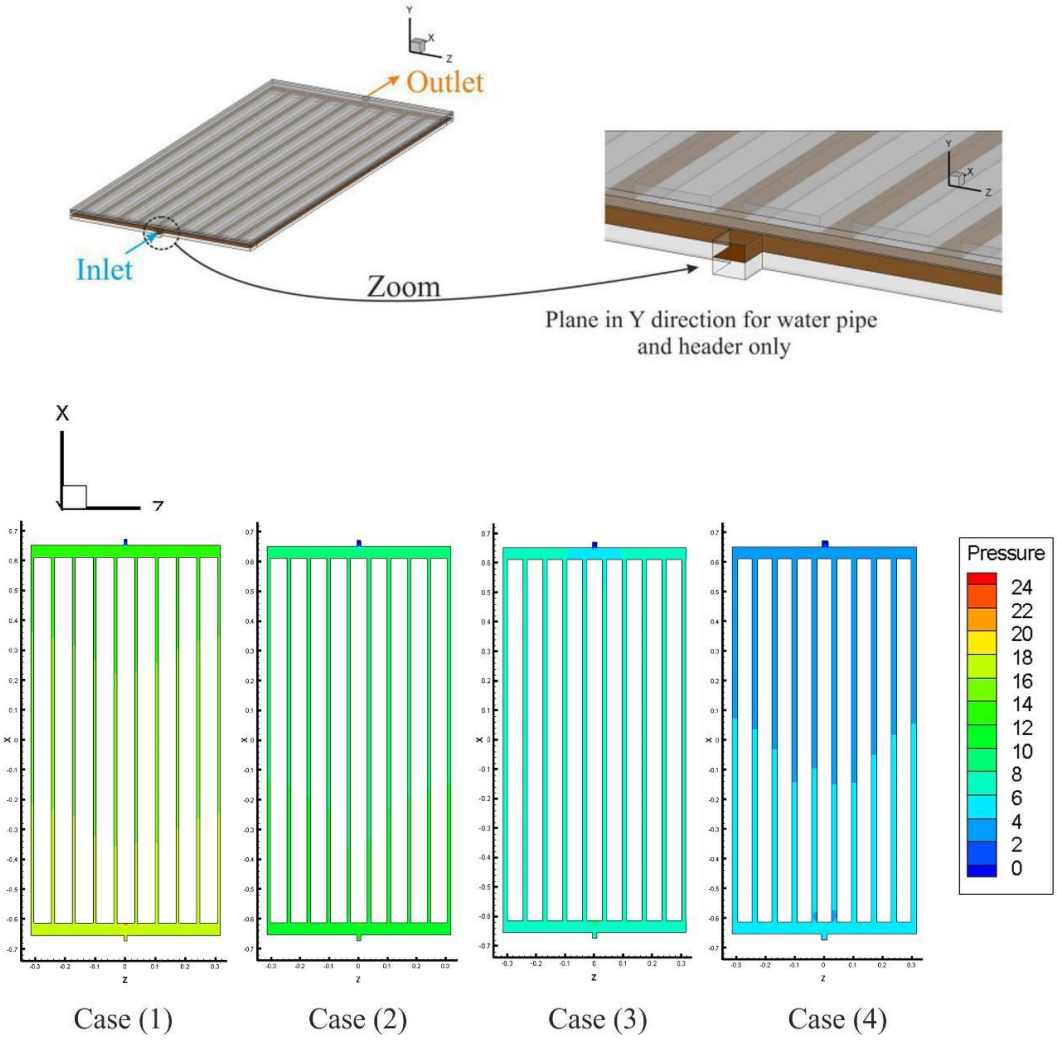

Figure 4.22. Distributions of pressure in cooling channels for Re 1200.

Re=1520

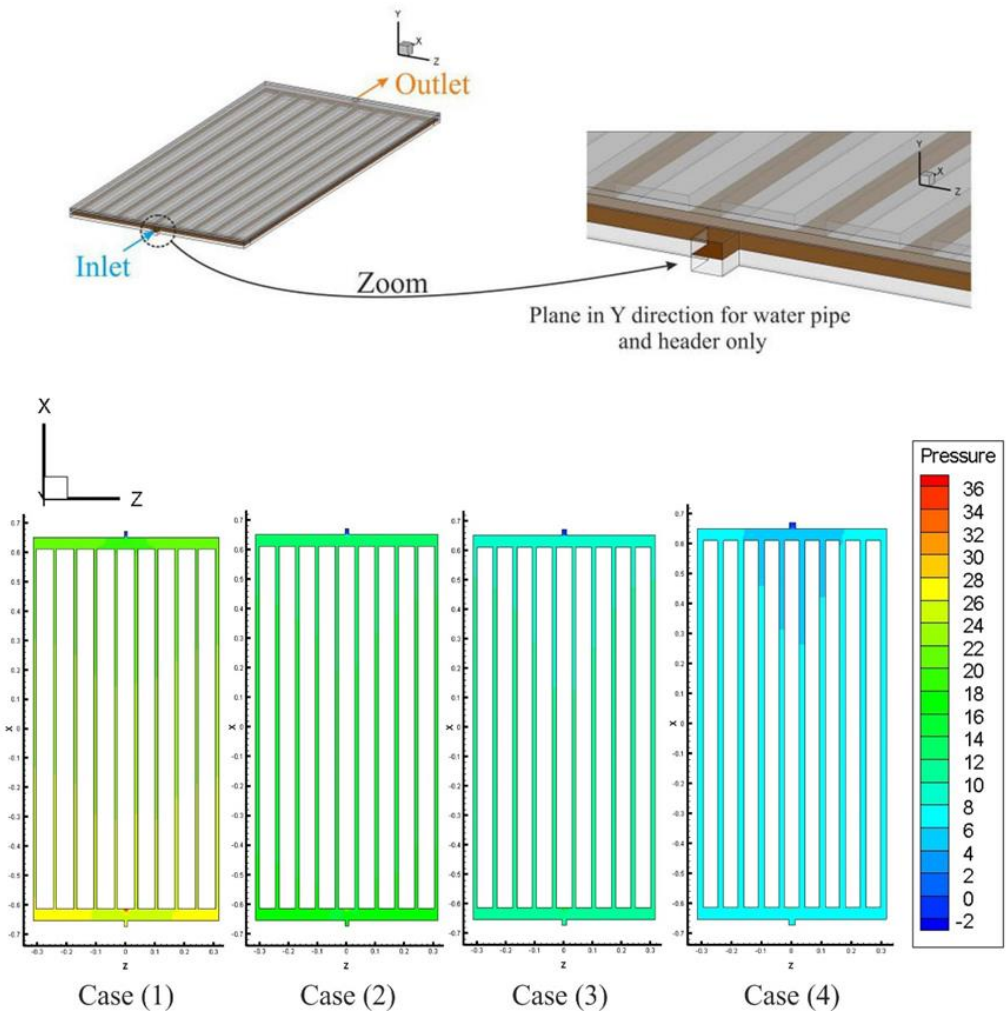

Figure 4.23. Distributions of pressure in cooling channels for Re 1520.

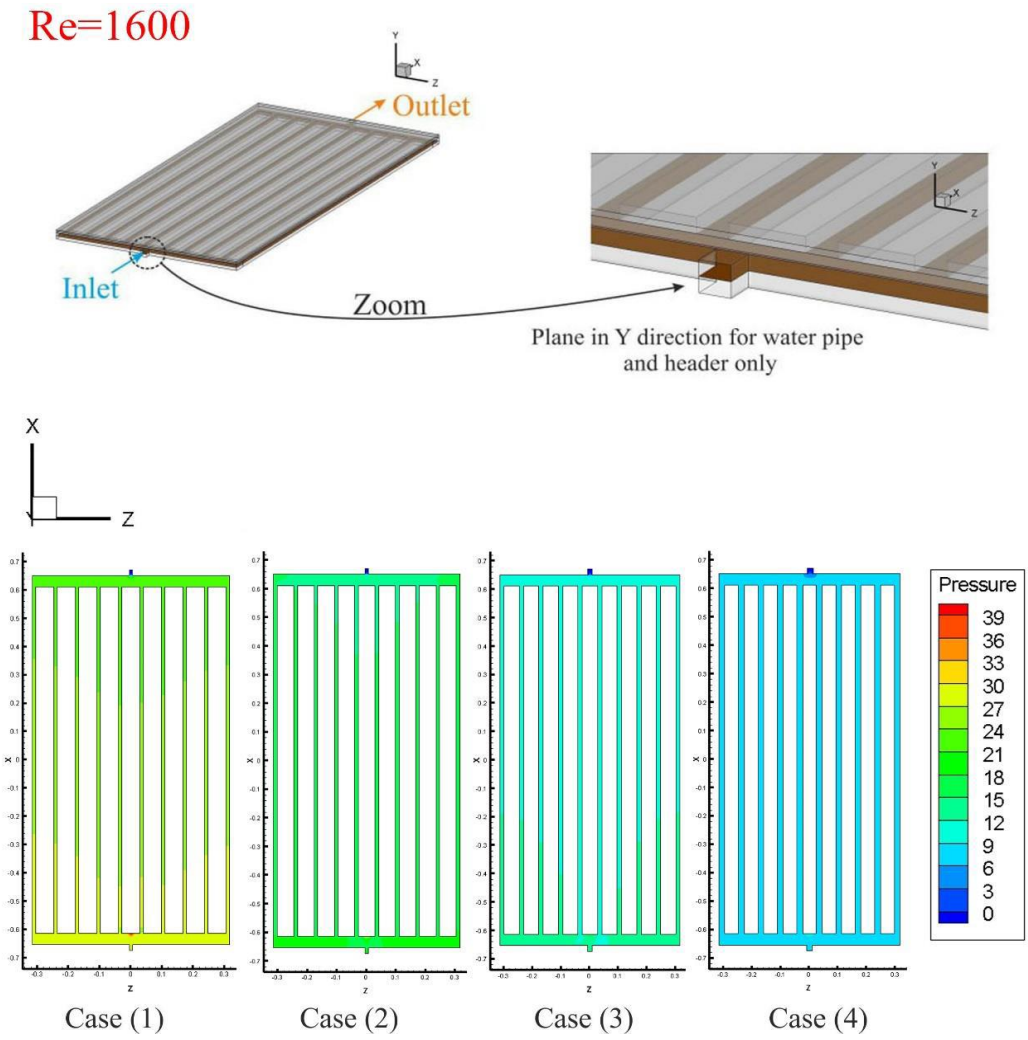

Figure 4.24. Distributions of pressure in cooling channels for Re 1600.

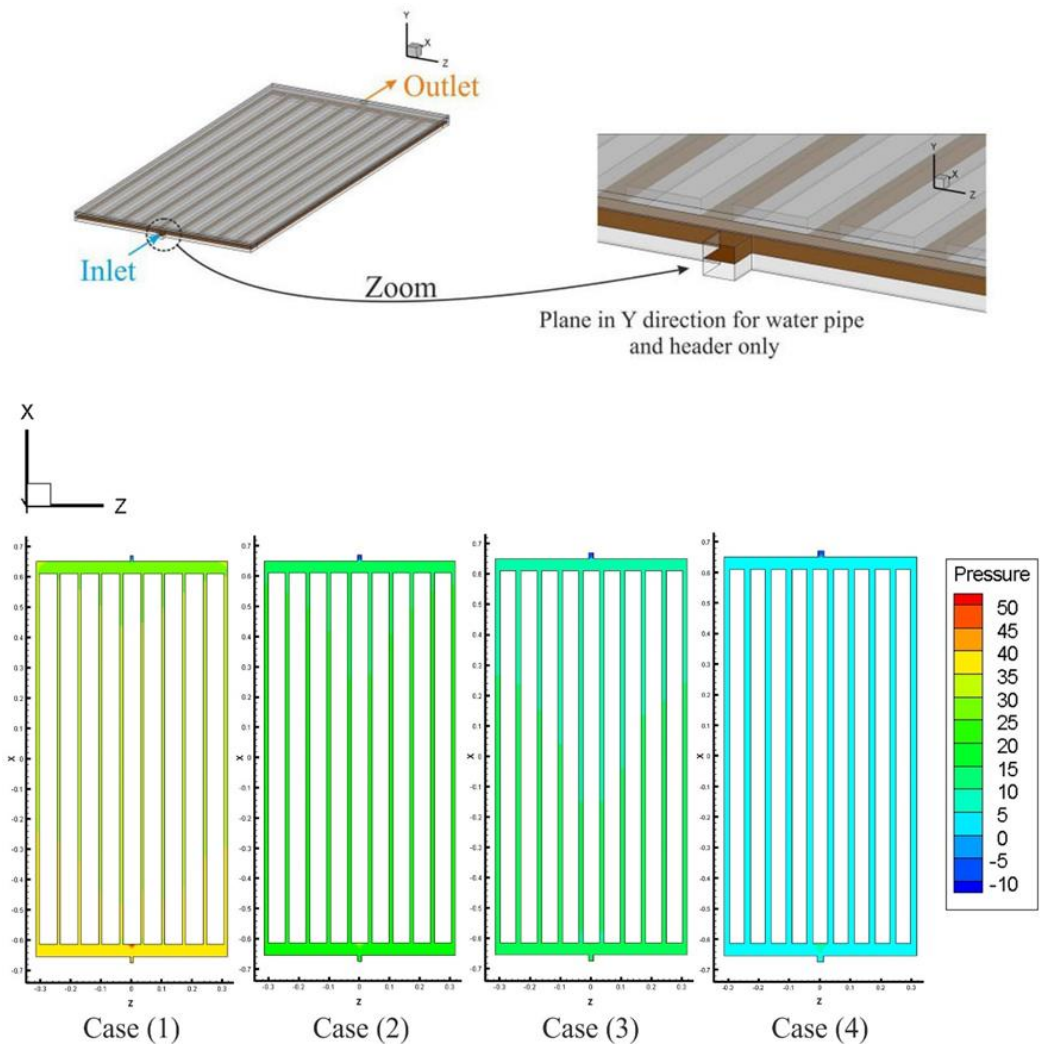

Figure 4.25. Distributions of pressure in cooling channels for Re 1850.

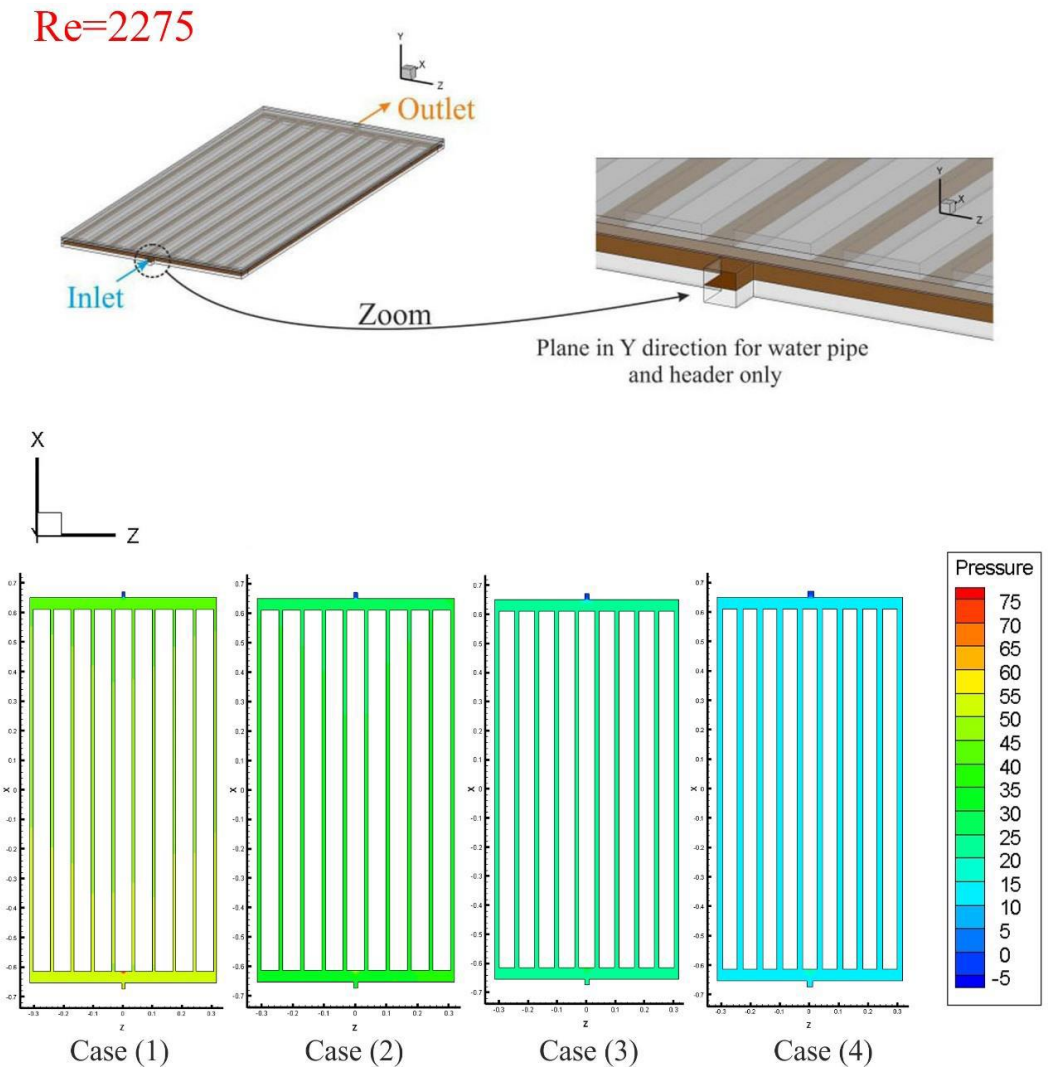

Figure 4.26. Distributions of pressure in cooling channels for Re 2275.

Figure 4.27 portrays the pressure drop in channels for the four cases of dimensions, and this figure shows that the pressure drop is low in the case of sub channel dimension (20*20); for example, with Re=1520, the pressure drop was 6.993 Pa for the fourth case, while this value for the other cases was 27.97 Pa, 17.497 Pa and 11.948 Pa, respectively. From the pressure drop curves, we can gain pressure drop lower by about 20.98 Pa if we compare between the fourth and first case, 4.952 Pa between the second and third case, and 10.48 Pa between the third and fourth case.

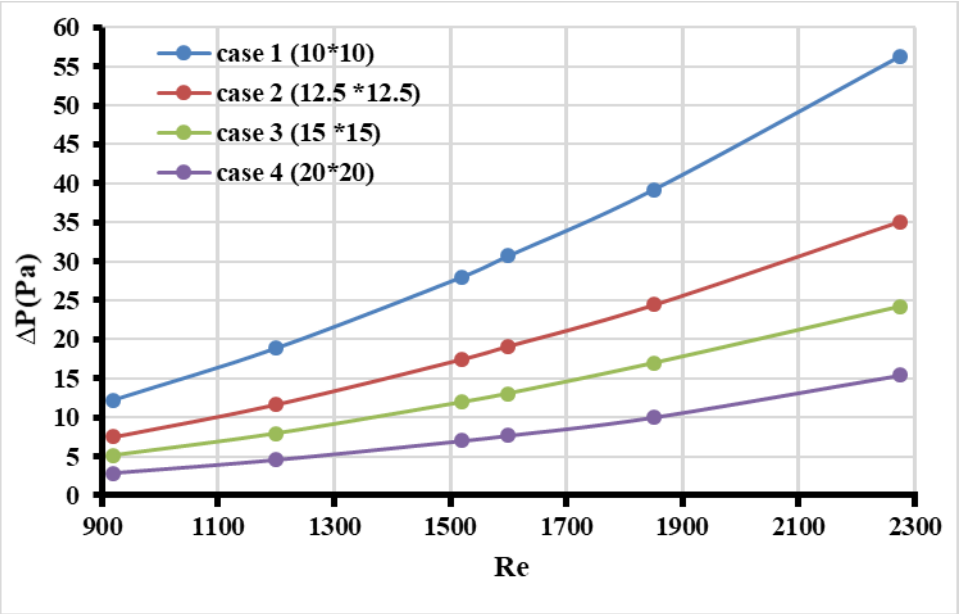

Figure 4.27. The pressure drop in the various dimensions of the cooling channels.

Figure 4.28 views that when the speed increases, the pressure drop increases too, and this increase in the pressure drop can be explained by the increase in friction resistance when the speed increases. In the case of sub channels dimension 10*10 the pressure drop increased from 12.19 Pa to 56.32 Pa, for the other case 12.5*12.5 of the dimension of sub channels, the pressure drop increased from 7.56 Pa to 35.3 Pa when Re changed from 920 to 2275, and for the case 15*15 dimension of sub channels, the pressure drop increased from 5.1 Pa to 24.72 Pa in the same range of Re values. When the sub channels had the dimension of 20*20, the pressure drop was the lowest where it ranged from 2.85 Pa to 14.65 Pa.

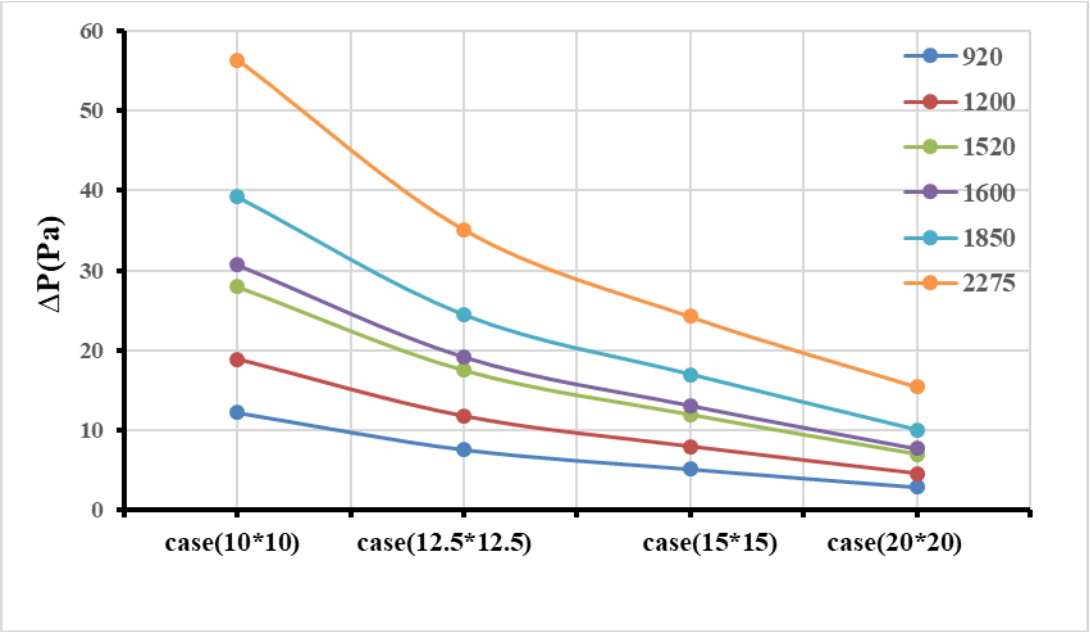

Figure 4.28. Pressure drops with Re number variation.

4.4. EFFECT OF THE SUB CHANNEL DIMENSION ON THE RATE HEAT TRANSFER TO THE COOLING WATER

Figure 4.29 depicts the heat transfer rate in the four cases of change in dimensions' sub channels (10*10), (12.5*12.5), (15*15), and (20*20) mm for Reynolds numbers (Re) (920,1200,1520,1600,1850 and 2275), it can be noted that the heat transfer rate increases with increasing Reynolds number, and in the first and second cases the heat transfer rate is higher because the smaller sub channels dimensions due to increased velocity. While, in the third and fourth cases, which have a larger dimension, the rate of heat transfer is lower due to the decrease in velocity within the channels. As the temperature difference increases, we observe that the rate of heat transfer also increases.

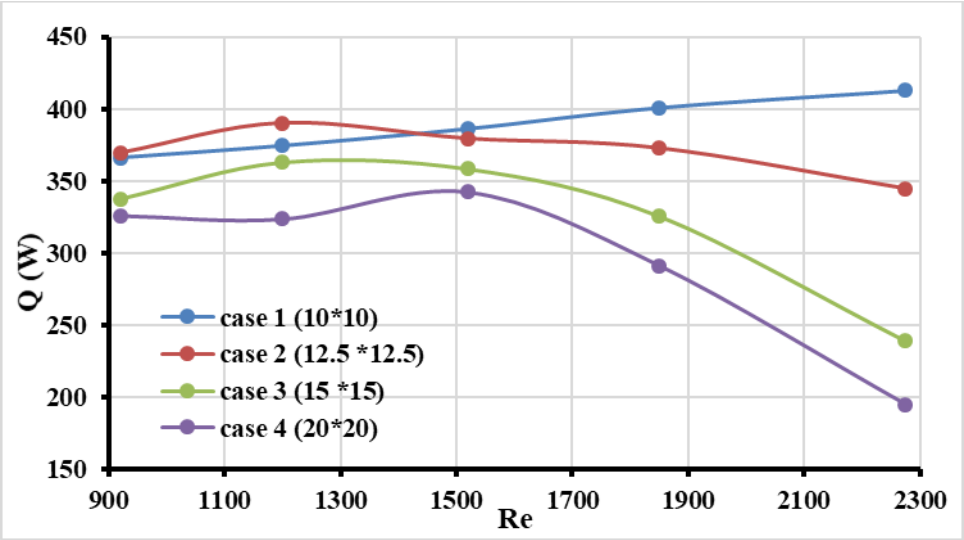

Figure 4.29. The rate of heat transfers in four cases with deferent Re numbers.

Figure 4.30 reveals the relation between the figure of merit (FoM) and Reynolds number for the four cases of the sub channel diameters (10*10), (12.5*12.5), (15*15), and (20*20) mm. The (FoM) declines with increasing Reynold number from 920 to 2275. The sub channel has the lowest pressure drop when its dimensions are 20 by 20, and a smaller pressure drop raises the (FoM), because it is inversely related to the pressure drop.

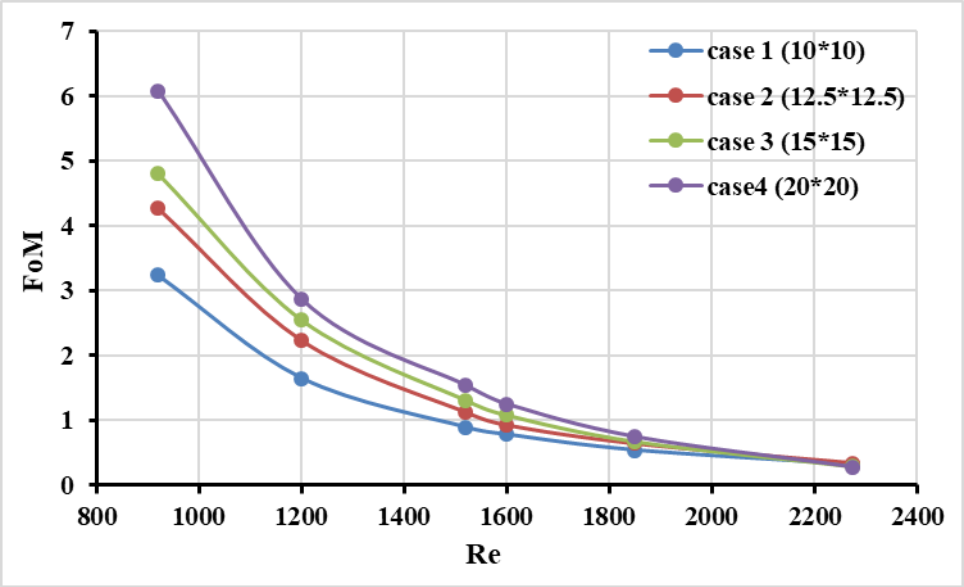

Figure 4.30. The figure of merit (FoM) with deferent Reynolds number.

PART 5

CONCLUSION

In this study, four different geometric modules were created employing Solid works, and simulation analyses were made by ANSYS Fluent software using various sub cooling channels (10×10) mm, (12.5×12.5) mm, (15×15) mm, and (20×20) mm on PVT collectors as well as compared with each other, to indicate the impact of sub cooling channels' dimensions on the thermal efficiency of PVT collector. The results manifested that the PV surface temperature decreases as the dimension of sub cooling channel increases, according to the results in the case (12.5×12.5) mm dimension for sub cooling channel, the average temperature of the PV surface was lower by about 4.18% compared to the first case which presents the (10×10) mm dimension, and for the third case (15×15) mm the average temperature of PV surface was lower by about 6.66%. In the case of (20×20) mm, the average temperature was 10% lower compared to the first case. For the pressure drop, if one compares the cases with the first case, the results will be: In the second case, the pressure drop is lower by about 37.68%, 57.22% in the third case, and 80.55% in the fourth case.

REFERENCES

1. Abdallah, S. R., Saidani-Scott, H., and Abdellatif, O. E., "Performance analysis for hybrid PV/T system using low concentration MWCNT (water-based) nanofluid", ***Solar Energy***, 181 (January): 108–115 (2019).

2. Aberoumand, S., Ghamari, S., and Shabani, B., "Energy and exergy analysis of a photovoltaic thermal (PV/T) system using nanofluids: An experimental study", ***Solar Energy***, 165 (January): 167–177 (2018).

3. El Hammoumi, A., Chtita, S., Motahhir, S., and El Ghzizal, A., "Solar PV energy: From material to use, and the most commonly used techniques to maximize the power output of PV systems: A focus on solar trackers and floating solar panels", ***Energy Reports***, 8: 11992–12010 (2022).

4. Internet: REN21, "What Are the Current Trends in Renewable Energy?", **https://www.ren21.net/what-are-the-current-trends-in-renewable-energy/**

5. Rypkema, H. A., "Environmental Chemistry, Renewable Energy, and Global Policy", ***Green Chemistry: An Inclusive Approach***, 19–47 (2018).

6. Kannan, N. and Vakeesan, D., "Solar energy for future world: - A review", ***Renewable And Sustainable Energy Reviews***, 62: 1092–1105 (2016).

7. Shankarappa, N., Ahmed, M., Shashikiran, N., and Naganagouda, D. H., "Solar Photovoltaic Systems – Applications & Configurations", ***International Research Journal Of Engineering And Technology(IRJET)***, 4 (8): 1851–1855 (2017).

8. Siah Chehreh, S., "An enviroeconomic review of the solar PV cells cooling technology effect on the CO2 emission reduction", ***Solar Energy***, 216 (November 2020): 468–492 (2021).

9. Brooks, A. E., "Solar Energy: Photovoltaics", Future Energy, 2. Ed., ***Elsevier***, USA, 383–404 (2014).

10. Mesquita, D. D. B., Lucas De Silva, J., Moreira, H. S., Kitayama, M., and Villalva, M. G., "A review and analysis of technologies applied in PV modules", ***2019 IEEE PES Conference On Innovative Smart Grid Technologies, ISGT Latin America 2019***, (2019).

11. Internet: Solar Energy Technologies Office, "Solar Photovoltaic Cell Research Directions", **https://www.energy.gov/eere/solar/articles/pv-cells-101-part-2-solar-photovoltaic-cell-research-directions** .

12. Joshi, S. S. and Dhoble, A. S., "Photovoltaic -Thermal systems (PVT): Technology review and future trends", ***Renewable And Sustainable Energy Reviews***, 92 (September 2017): 848–882 (2018).

13. Herez, A., El, H., Lemenand, T., and Ramadan, M., "Review on photovoltaic / thermal hybrid solar collectors : Classi fi cations , applications and new systems", 207 (February): 1321–1347 (2020).

14. Laghari, I. A., Samykano, M., Pandey, A. K., Kadirgama, K., and Tyagi, V. V., "Advancements in PV-thermal systems with and without phase change materials as a sustainable energy solution: energy, exergy and exergoeconomic (3E) analytic approach", ***Sustainable Energy And Fuels***, 4 (10): 4956–4987 (2020).

15. Vaishak, S. and Bhale, P. V., "Photovoltaic/thermal-solar assisted heat pump system: Current status and future prospects", ***Solar Energy***, 189 (July): 268–284 (2019).

16. Pathak, S. K., Sharma, P. O., Goel, V., Bhattacharyya, S., Aybar, H. Ş., and Meyer, J. P., "A detailed review on the performance of photovoltaic/thermal system using various cooling methods", ***Sustainable Energy Technologies And Assessments***, 51: 101844 (2022).

17. Abdul Hamid, S., Yusof Othman, M., Sopian, K., and Zaidi, S. H., "An overview of photovoltaic thermal combination (PV/T combi) technology", ***Renewable And Sustainable Energy Reviews***, 38: 212–222 (2014).

18. Lamnatou, C. and Chemisana, D., "Photovoltaic/thermal (PVT) systems: A review with emphasis on environmental issues", ***Renewable Energy***, 105: 270–287 (2017).

19. Sultan, S. M. and Ervina Efzan, M. N., "Review on recent Photovoltaic/Thermal (PV/T) technology advances and applications", ***Solar Energy***, 173 (August): 939–954 (2018).

20. Yu, Q., Chen, X., and Yang, H., "Research progress on utilization of phase change materials in photovoltaic/thermal systems: A critical review", ***Renewable And Sustainable Energy Reviews***, 149 (August 2020): (2021).

21. Daghigh, R., Ruslan, M. H., and Sopian, K., "Advances in liquid based photovoltaic/thermal (PV/T) collectors", ***Renewable And Sustainable Energy Reviews***, 15 (8): 4156–4170 (2011).

22. Rejeb, O., Gaillard, L., Giroux-Julien, S., Ghenai, C., Jemni, A., Bettayeb, M., and Menezo, C., "Novel solar PV/Thermal collector design for the enhancement of thermal and electrical performances", ***Renewable Energy***, 146: 610–627 (2020).

23. Arslan, E., Aktaş, M., and Can, Ö. F., "Experimental and numerical investigation of a novel photovoltaic thermal (PV/T) collector with the energy and exergy

analysis", ***Journal Of Cleaner Production***, 276: (2020).

24. Elbreki, A. M., Sopian, K., Fazlizan, A., and Ibrahim, A., "An innovative technique of passive cooling PV module using lapping fins and planner reflector", ***Case Studies In Thermal Engineering***, 19 (February): 100607 (2020).

25. Elbreki, A. M., Muftah, A. F., Sopian, K., Jarimi, H., Fazlizan, A., and Ibrahim, A., "Experimental and economic analysis of passive cooling PV module using fins and planar reflector", ***Case Studies In Thermal Engineering***, 23 (November 2020): 100801 (2021).

26. Boumaaraf, B., Touafek, K., Ait-cheikh, M. S., and Slimani, M. E. A., "Comparison of electrical and thermal performance evaluation of a classical PV generator and a water glazed hybrid photovoltaic–thermal collector", ***Mathematics And Computers In Simulation***, 167: 176–193 (2020).

27. Choubineh, N., Jannesari, H., and Kasaeian, A., "Experimental study of the effect of using phase change materials on the performance of an air-cooled photovoltaic system", ***Renewable And Sustainable Energy Reviews***, 101 (April 2018): 103–111 (2019).

28. Javidan, M. and Moghadam, A. J., "Experimental investigation on thermal management of a photovoltaic module using water-jet impingement cooling Design of Experiment", 228 (July 2020): (2021).

29. Khaled, S. and Ali, O., "Numerical and experimental investigation for hybrid photovoltaic/thermal collector system in Duhok city", ***Journal Of Environmental Engineering And Landscape Management***, 28 (4): 202–212 (2020).

30. Keen, V. I. and Prajapati, S., "Experimental Analysis of Evacuated Tube Solar Water Heater Using Twisted Tape", 5 (12): 181–187 (2018).

31. Selimli, S., Dumrul, H., Yilmaz, S., and Akman, O., "Experimental and numerical analysis of energy and exergy performance of photovoltaic thermal water collectors", ***Solar Energy***, 228 (August): 1–11 (2021).

32. Poredoš, P., Tomc, U., Petelin, N., Vidrih, B., Flisar, U., and Kitanovski, A., "Numerical and experimental investigation of the energy and exergy performance of solar thermal, photovoltaic and photovoltaic-thermal modules based on roll-bond heat exchangers", ***Energy Conversion And Management***, 210 (March): (2020).

33. Rosli, M. A. M., Ping, Y. J., Misha, S., Akop, M. Z., Sopian, K., Mat, S., Al-Shamani, A. N., and Saruni, M. A., "Simulation study of computational fluid dynamics on photovoltaic thermal water collector with different designs of absorber tube", ***Journal Of Advanced Research In Fluid Mechanics And Thermal Sciences***, 52 (1): 12–22 (2018).

34. Zhou, J., Ke, H., and Deng, X., "Experimental and CFD investigation on temperature distribution of a serpentine tube type photovoltaic/thermal collector", ***Solar Energy***, 174 (September): 735–742 (2018).

35. Misha, S., Abdullah, A. L., Tamaldin, N., Rosli, M. A. M., and Sachit, F. A., "Simulation CFD and experimental investigation of PVT water system under natural Malaysian weather conditions", ***Energy Reports***, 6: 28–44 (2020).

36. Salem, M. R., Ali, R. K., and Elshazly, K. M., "Experimental investigation of the performance of a hybrid photovoltaic/thermal solar system using aluminium cooling plate with straight and helical channels", ***Solar Energy***, 157: 147–156 (2017).

37. Kazem, H. A., "Case Studies in Thermal Engineering Evaluation and analysis of water-based photovoltaic / thermal (PV / T) system", ***Case Studies In Thermal Engineering***, 13 (January): 100401 (2019).

38. Engin, D. and Çolak, M., "Modeling and performance optimization of photovoltaic and thermal collector hybrid system", ***Turkish Journal Of Electrical Engineering And Computer Sciences***, 24 (5): 3524–3542 (2016).

39. Khelifa, A., Touafek, K., Ben Moussa, H., and Tabet, I., "Modeling and detailed study of hybrid photovoltaic thermal (PV/T) solar collector", ***Solar Energy***, 135: 169–176 (2016).

40. Michael, J. J. and Selvarasan, I., "Experimental investigation of a copper sheet-laminated solar photovoltaic thermal water collector", ***Energy Efficiency***, 10 (1): 117–128 (2017).

41. Shen, C., Liu, F., Qiu, S., Liu, X., Yao, F., and Zhang, Y., "Numerical study on the thermal performance of photovoltaic thermal (PV/T) collector with different parallel cooling channels", ***Sustainable Energy Technologies And Assessments***, 45 (July 2020): (2021).

42. Ul Abdin, Z., Rachid, A., and Korkut, T. B., "Design and analysis of an innovative photovoltaic-thermal collector with embedded tank", ***Solar Energy***, 245 (May): 290–298 (2022).

43. Bria, A., Raillani, B., Chaatouf, D., Salhi, M., Amraqui, S., and Mezrhab, A., "Optimization and analysis of a hybrid thermal photovoltaic collector: Thermal and electrical investigation", ***Energy For Sustainable Development***, 71: 573–584 (2022).

44. Chen, Y., Zhang, C., Shi, M., and Yang, Y., "Thermal and hydrodynamic characteristics of constructal tree-shaped minichannel heat sink", ***AIChE Journal***, 56 (8): 2018–2029 (2010).

45. Su, D., Jia, Y., Huang, X., Alva, G., Tang, Y., and Fang, G., "Dynamic performance analysis of photovoltaic-thermal solar collector with dual channels

for different fluids", ***Energy Conversion And Management***, 120: 13–24 (2016).

46. Liang, S., Zheng, H., Liu, S., and Ma, X., "Optical design and validation of a solar concentrating photovoltaic-thermal (CPV-T) module for building louvers", ***Energy***, 239: (2022).

47. Dubey, S. and Tay, A. A. O., "Testing of two different types of photovoltaic-thermal (PVT) modules with heat flow pattern under tropical climatic conditions", ***Energy For Sustainable Development***, 17 (1): 1–12 (2013).

48. Salman, A. H. A., Hilal, K. H., and Ghadhban, S. A., "Enhancing performance of PV module using water flow through porous media", ***Case Studies In Thermal Engineering***, 34 (January): 102000 (2022).

49. Prasetyo, S. D., Prabowo, A. R., and Arifin, Z., "The use of a hybrid photovoltaic/thermal (PV/T) collector system as a sustainable energy-harvest instrument in urban technology", ***Heliyon***, 9 (2): e13390 (2023).

50. Huide, F., Xuxin, Z., Lei, M., Tao, Z., Qixing, W., and Hongyuan, S., "A comparative study on three types of solar utilization technologies for buildings: Photovoltaic, solar thermal and hybrid photovoltaic/thermal systems", ***Energy Conversion And Management***, 140: 1–13 (2017).

51. Pang, W., Zhang, Q., Cui, Y., Zhang, L., Yu, H., Zhang, X., Zhang, Y., and Yan, H., "Numerical simulation and experimental validation of a photovoltaic/thermal system based on a roll-bond aluminum collector", ***Energy***, 187: (2019).

52. Kiwan, S., Al-Nimr, M., and Salim, I., "A hybrid solar chimney/photovoltaic thermal system for direct electric power production and water distillation", ***Sustainable Energy Technologies And Assessments***, 38 (November 2019): (2020).

53. Salari, A. and Hakkaki-Fard, A., "A numerical study of dust deposition effects on photovoltaic modules and photovoltaic-thermal systems", ***Renewable Energy***, 135: 437–449 (2019).

54. Lee, C. K., "Computational analysis of heat transfer in turbulent flow Past a horrizontal surface with two dimensional ribs", ***Elsevier Science***, 28 (2): 161–170 (2001).

55. Li, Y. and Nielsen, P. V., "Commemorating 20 years of Indoor Air: CFD and ventilation research", ***Indoor Air***, 21 (6): 442–453 (2011).

56. Pawar, V. R. and Sobhansarbandi, S., "CFD modeling of a thermal energy storage based heat pipe evacuated tube solar collector", ***Journal Of Energy Storage***, 30 (April): (2020).

57. Norton, T. and Sun, D. W., "Computational fluid dynamics (CFD) - an effective and efficient design and analysis tool for the food industry: A review", ***Trends In***

Food Science And Technology, 17 (11): 600–620 (2006).

58. El-Emam, M. A., Zhou, L., Shi, W., Han, C., Bai, L., and Agarwal, R., "Theories and Applications of CFD–DEM Coupling Approach for Granular Flow: A Review", Archives of Computational Methods in Engineering, ***Springer Netherlands***, 4979–5020 (2021).

59. Heris, S. Z., Esfahany, M. N., and Etemad, G., "Numerical investigation of nanofluid laminar convective heat transfer through a circular tube", ***Numerical Heat Transfer; Part A: Applications***, 52 (11): 1043–1058 (2007).

60. He, Y., Men, Y., Zhao, Y., Lu, H., and Ding, Y., "Numerical investigation into the convective heat transfer of TiO2 nanofluids flowing through a straight tube under the laminar flow conditions", ***Applied Thermal Engineering***, 29 (10): 1965–1972 (2009).

61. Bianco, V., Chiacchio, F., Manca, O., and Nardini, S., "Numerical investigation of nanofluids forced convection in circular tubes", ***Applied Thermal Engineering***, 29 (17–18): 3632–3642 (2009).

62. Chen, Y. and Deng, Z., "Hydrodynamics of a droplet passing through a microfluidic T-junction", ***Journal Of Fluid Mechanics***, 819 (May): 401–434 (2017).

63. Sun, D., Zhu, M., Pan, S., and Raabe, D., "Lattice Boltzmann modeling of dendritic growth in a forced melt convection", ***Acta Materialia***, 57 (6): 1755–1767 (2009).

64. Dai, W. J., Gan, Y. X., and Hanaor, D., "Effective Thermal Conductivity of Submicron Powders: A Numerical Study", ***Applied Mechanics And Materials***, 846: 500–505 (2016).

65. Cengel, Y. A., "HEAT TRANSFER A Practical Approach", 2. Ed., ***McGraw-Hill***, New York, 343 (2002).

RESUME

Zainab Mohemmed Sellab AL-MAMOORI is a Mechanical engineer. She completed her bachelor's degree at the University of Baghdad, Department of Mechanical Engineering in Baghdad 2006-2007. Then in 2021. Currently studying for a master’s degree at Karabuk University in the field of Mechanical Systems Engineering.